J. Min. Metall. Sect. B-Metall. 60 (2) (2024) 235 - 257

Journal of Mining and Metallurgy, Section B: Metallurgy

EFFECT OF CHROMIUM AND TITANIUM ON THE MICROSTRUCTURE AND MECHANICAL PROPERTIES OF CAST STEEL

B. Białobrzeska [a,*], R. Jasiński [a], R. Dziurka [b], P. Bała [b]

[a] Wroclaw University of Science and Technology, Faculty of Mechanical Engineering, Wrocław, Poland
[b] AGH University of Krakow, Faculty of Metals Engineering and Industrial Computer Science, Kraków, Poland

(Received 24 April 2024; Accepted 24 September 2024)

Abstract

In this work, the influence of chromium and titanium on the microstructure and mechanical properties of cast steel is investigated. The analysis was carried out on a material covered by patent Pat.243157. Advanced techniques were used, including dilatometric analysis, light microscopy (LM), scanning electron microscopy (SEM) and transmission electron microscopy (TEM). The material was examined in various states: as-cast, quenched, and quenched with subsequent tempering at 200 °C, 400 °C, and 600 °C. Important mechanical properties such as hardness, yield strength, percentage elongation, percentage reduction in area after fracture, and impact toughness at temperatures ranging from -40 °C to +20 °C were evaluated. The results were compared with those of a reference cast steel without these alloying elements, allowing a detailed assessment of the influence of chromium and titanium. The investigation begins with a comprehensive literature review of the effects of these elements in iron-based alloys. The results highlight the influence of chromium and titanium on the mechanical properties and microstructural development of cast steel. These elements play a critical role in enhancing mechanical strength, particularly after quenching and tempering, although there are evident trade-offs in ductility and impact toughness. In addition, the study discusses the damage mechanisms, focusing on the role of titanium nitrides in the cracking process.

Keywords: *Cast steel; Titanium; Chromium; Heat treatment; Microstructure; Mechanical properties*

1. Introduction

Chromium is commonly used as an alloying addition in iron-based alloys due to a range of special properties it imparts. According to the PN-EN 10020:2003 standard, the threshold chromium content, from which it is considered as an alloying addition, is 0.3% by weight. Literature review revealed that chromium is essentially found in all alloy steels. The concentration in various steel groups is as follows: general-purpose structural alloy steels ≤2.6%, for pressure and room and elevated temperature operation ≤17% by weight, for pressure and low temperature operation ≤13.5% by weight, wear-resistant structural steels ≤2.5%, heat-resistant and high-temperature steels, including high-chromium steels 6-30% by weight, ferritic-austenitic 25-28% by weight, and austenitic 16-27% by weight, as well as martensitic corrosion-resistant steels 11.5-17% by weight, austenitic 18-26% by weight, and austenitic-ferritic 21-27% by weight [1]. In wear-resistant steels, it is usually present in amounts up to 2% by weight [2]. Furthermore, high-chromium alloys are widely used for cladding wear-prone industrial components in mining, cement plants, thermal power plants, and in the iron and steel industry due to their high wear resistance, attributed to the formation of chromium carbides [3–5]. Due to significant changes in the kinetics of transformations during heating and cooling caused by the addition of chromium, several research works focus particularly on this aspect. It was observed that the addition of at least 5% by weight of chromium, in combination with manganese, reduces the critical cooling rate to such an extent that it allows the steel to be air-hardened [6]. It was noted that an addition of less than 1% by weight of chromium in dual-phase (DP) steels delays the bainitic transformation [7]. The impact of chromium on the properties of steel subjected to Q&P treatment (quenching and partitioning) was also analyzed [8]. In the course of the studies, it was found that 42SiCr steel containing 1.33% by weight of chromium is less sensitive to changes in process parameters, thereby a desired microstructure with a strength higher than

Corresponding author: beata.bialobrzeska@pwr.edu.pl

https://doi.org/10.2298/JMMB240424023B

1900 MPa and a relative elongation of at least 15% can be achieved over a wide range of parameters. Steel of similar chemical composition but devoid of chromium addition showed greater sensitivity to variations in temperature-time variables, limiting the possibility of obtaining a martensitic microstructure with partial austenite without the presence of ferrite, resulting in a decrease in strength properties by 700 MPa. It was established that the strength properties of steel increase by 100 MPa for every 1% by weight of chromium in the alloy. Given that chromium is a carbide-forming element, it is also necessary to be aware of the changes it causes during tempering, especially at temperatures where its diffusion and redistribution between the matrix and carbides are possible. In the work of Dąbrowski and Pacyna [9], a quantitative assessment of the impact of chromium on the transformations occurring at the early stage of tempering of hypereutectoid steels was made. The subject of the study was unalloyed steel C110 and steel 115Cr5 containing 1.15% by weight of carbon and 1.23% by weight of chromium. It was shown that dissolving 1.23% chromium in austenite practically does not affect the starting temperature of the ε_s contraction (likely associated with the precipitation of ε carbide) occurring at the early stage of tempering, but raises both the end temperature of the ε_f contraction and its maximum intensity ε_{max}. Furthermore, it was demonstrated that the plane strain fracture toughness (K_{IC}) of low-tempered (at 200 °C) C110 steel, after prior hardening from the homogenous austenite range, is greater than that of alloy steel 115Cr5. Zikeev [10] suggested that in the case of steels containing molybdenum and vanadium, the addition of chromium should reduce susceptibility to tempering. In the course of conducted studies, he reached different conclusions than Pacyna and Dąbrowski [9]. Namely, he noticed that during low tempering (at 200 °C), chromium did not have a significant impact on the mechanical properties (strength and plasticity), whose values were similar to those of steel without chromium. Subsequently, with the increase in tempering temperature, there was a decrease in hardness regardless of the considered concentrations of this element. After tempering at 550 °C, there was an increase in strength properties as a result of processes related to precipitation hardening, allowing the observation of the hardening effect of chromium. With an increase in chromium content from 0.5 to 3% by weight, there was an increase in tensile strength from 1480 MPa to 1600 MPa, yield strength from 1310 MPa to 1380 MPa, with a simultaneous deterioration in ductility. It should be noted that the greatest effect of chromium was observed for a content of 2% by weight, while at higher contents of this element, the increases in strength parameters were not as spectacular. During tempering at higher temperatures, the presence of chromium caused the precipitation of type $(M)_{23}C_6$ carbides, resulting in the occurrence of secondary hardening effect [11].

Interactions of chromium with other elements have also been analyzed [3, 11–16], with titanium [11]. Titanium belongs to the group of elements that form carbides and nitrides. It creates very hard titanium carbides (TiC) that are stable up to 1050 °C [17]. It also limits the solubility of nitrogen in the solid solution by binding it in the form of nitrides such as TiN (less commonly Ti_2N), which are partially formed during crystallization in interdendritic spaces, and subsequently in austenite, also in the form of Ti(C,N), which are more stable than vanadium or aluminum nitrides. Furthermore, it has been observed that TiN type nitrides can be stable up to temperatures of 1100-1200 °C, making them excellent grain growth inhibitors, especially in high-temperature technological processes, such as welding. Titanium nitride precipitates are regular parallelepipeds with sharp edges, which easily nucleate and grow into larger particles often near non-metallic inclusions [18, 19], e.g., MnS, Al_2O_3, MgO. The addition of titanium reduces the ductility of the material when cooled at high rates, an effect that can be mitigated by reducing the amount of nitrogen and aluminum [20]. It has been found that the ductility of steel containing niobium and additionally titanium improves with a decrease in cooling rate, an increase in the size of titanium-rich precipitates, with a simultaneous decrease in their volumetric fraction in the microstructure. It has been demonstrated that the presence of finer precipitates invariably results in poorer ductility, possibly because cracks more readily join along the boundaries if these precipitates are close to each other [21]. Precipitation hardening can be achieved through the precipitation of TiC carbides of nanometer size in ferrite. However, the precipitation of titanium carbides and nitrides of micron-sized particles can lead to cracks, particularly reducing impact toughness at lowered temperatures and the fatigue strength of steel [22–25], as well as increasing susceptibility to hydrogen embrittlement [26]. Laboratory works on steels containing titanium indicate that particles with sufficient dispersion, providing satisfactory ductility, only form at relatively slow cooling [20, 27]. In steel containing niobium, a significant improvement in ductility was noted during cooling at a rate of 25 K/min. The analysis of the precipitates suggests that at such a cooling rate, niobium may precipitate on coarse-

grained titanium nitrides. Meanwhile, in aluminum-added steels cooled at a rate of 60 K/min, a slight improvement in ductility caused by the presence of titanium was observed, regardless of the carbon content. It is believed that this improvement was due to the precipitation of nitrogen from the solution by titanium and preventing the precipitation of aluminum nitrides AlN [27]. Given that this article undertakes the characterization of steel with chromium and titanium, the analysis of the interactions between these two elements is particularly important. Zhang et al. [28, 29], studying the effect of chromium addition on the microstructure and properties of welded TiC-VC coatings reinforced with Fe, found that the welded layer with 3.0% by weight of chromium had the highest microhardness of 1090 HV0.2, and the welded layer with 12.0% by weight of chromium showed the best corrosion resistance. Matveeva [30] undertook an evaluation of the comprehensive impact of chromium and titanium on the microstructure and properties of white cast irons. The results of the study led to the conclusion that titanium neutralizes the carbide-forming action of chromium in the studied concentration ranges, i.e., from 1.17 to 5.63% by weight. In the presence of titanium, the effect of chromium on hardness was lesser in comparison to its individual action, which was manifested by the following result: the addition of chromium alone increased the hardness of the experimental samples 2.1 times, in combination with 0.2% by weight of titanium - only by 1.1 times, and with 0.01% by weight of titanium, the increase in chromium content did not affect the hardness. The impact of titanium content on the microstructure and properties of high-manganese steel with chromium [31] was also analyzed. The study found that the micro-addition of titanium caused, among other effects, grain refinement, an increase in hardness by 87-263%, an improvement in wear resistance, while simultaneously causing a decrease in tensile strength.

The conducted literature review revealed limited access to data analyzing the synergistic effect of chromium and titanium on the microstructural and mechanical properties of medium-carbon steels. Therefore, in the course of our own research, such an analysis was conducted, including the design and production of steel with the appropriate chemical composition, carrying out heat treatment involving standard thermal procedures, and testing mechanical properties, including tensile testing and impact tests at room and reduced temperatures.

2. Experimental

The material for the study was a low-alloy cast steel developed by the authors of this paper and patented under the number: Pat.243157. The chemical composition of the analyzed material is presented in the Table 1. Chromium and titanium were specifically chosen as alloying elements due to their significant impact on the steel's properties. Chromium substantially increases the hardenability of the steel, which is crucial for achieving the desired mechanical properties through heat treatment processes. Titanium was included for its effectiveness in refining the grain structure and forming stable carbides and nitrides, which contribute to enhanced strength of the material. These alloying elements were selected to achieve a balance between hardness, strength, and toughness, ensuring that the developed steel meets the performance requirements for demanding applications.

Molds for ingots were made in bentonite mass using wooden models. Melting was carried out in a Radyne type medium frequency induction furnace with a capacity of 100 kW, 120 kg, and neutral lining. The charge mass was approximately 110 kg each time. A hood was mounted over the crucible, under which argon was blown to maintain the desired chemical composition. The chemical composition was analyzed using an ARL NA optical emission spectrometer with spark excitation, except for elements in minimal amounts determined by atomic absorption spectrometry using the Solaar M6 Thermo device.

Rectangular samples were taken from the ingots, which were subjected to preliminary heat treatment, consisting of homogenizing annealing (austenitizing temperature – 1200 °C, austenitizing time – 1h, cooling with the furnace), and then normalizing (austenitizing temperature – 900 °C, austenitizing time – 1h, air cooling). The above heat treatment was carried out in an argon protective atmosphere in a conventional FCF 12 SHM/R furnace with a gas-tight retort. From such thermally treated material, cylindrical samples of standardized dimensions Ø3 mm x 10 mm were made, which were subjected to dilatometric studies. Dilatometric studies were

Table 1. *Chemical composition of the analyzed steel, % by weight (nitrogen in ppm)*

C	Si	Mn	P	S	Cr	Ni
0.30	0.41	1.45	0.017	0.010	1.000	0.112
Mo	Cu	V	Ti	Al	B	N
0.029	0.110	0.013	0.059	0.039	0.0003	161

performed using a Linseis L78 RITA dilatometer. Austenitizing temperatures were selected after preliminary dilatometric studies, in which the Ac_3 temperature was determined. The austenitizing temperature was 50 °C higher than the Ac_3 temperature and amounted to 890 °C. Samples were heated at a rate of 5 ºC/s and then cooled at different rates $V_{800\text{-}500}$, recording changes in the elongation of the samples depending on the temperature. Digital registration of dilatograms allowed their differentiation to accurately determine the temperatures of subsequent transformations. Based on the characteristic points read from the differential curves, CCT graphs were made.

Microscopic examinations were carried out using a Nikon ECLIPSE MA200 light microscope (LM) and Phenom XL scanning electron microscopes (SEM) with backscattered electron (BSE) or secondary electron detector (SED) contrast, and an accelerating voltage of 15 kV, as well as a Versa 3D microscope (Everhart-Thornley detector ETD, accelerating voltage 20 kV). Microstructures were revealed using etchant 74 (5% HNO_3 solution in alcohol) according to ASTM E407 standard. Additional observations of the microstructure were conducted using transmission electron microscopy (TEM) with a Tecnai G2 20 TWIN (FEI) microscope. The sample preparation included the production of thin foils using Ga+ ions with a Quanta 3D 200i FIB device from FEI equipped with an ion column based on a scanning microscope.

Hardness measurements were conducted using the static Brinell method in accordance with the EN ISO 6506-1:2014-12 standard and the Vickers method according to the EN ISO 6507-1:2018-05 standard. For the Brinell method, a Zwick/Roell ZHU hardness tester was used, with a 2.5 mm diameter ball and a load of 187.5 kg applied for 15 seconds. Vickers hardness measurements were performed using a Tukon hardness tester with a load of 49 N.

The tensile test at room temperature was conducted based on the currently valid standard EN ISO 6892-1:2019. The experiments were carried out on an Instron 5982 tensile testing machine along with an extensometer with a specified gauge length of L_0 = 25 mm. The test series consisted of 4 samples for all considered material states. The tensile test was conducted at a constant strain rate controlled based on the rate of stress increase (method B according to the mentioned standard) until break. Basic strength properties of the material were determined: the proof strength or yield strength (R_e or $R_{p0.2}$) and tensile strength (R_m), as well as plastic properties: percentage elongation after fracture (A) and percentage reduction of area after fracture (Z). For the purposes of the tests, typical proportional samples for this type of strength test were made with a circular cross-section and a diameter of d = 10 mm and a gauge length of L_0 = 50 mm. Samples were taken symmetrically distributed across the section of the ingot, maintaining the direction of the sample axis aligned with the longitudinal axis of the ingot, and surface layers of the ingot material containing surface defects resulting from the casting technology were discarded. The measurement results were averaged, and confidence intervals and standard deviation were determined according to the t-Student distribution.

Impact tests using the Charpy method were conducted using a Zwick Roell RPK300 pendulum impact tester, applying an initial energy value of 300 J, in accordance with the standard PN-EN ISO 148-1:2017-02. Rectangular samples with “V” notches were used for the tests. Samples were taken symmetrically distributed across the section of the ingot, maintaining the direction of the sample axis aligned with the longitudinal axis of the ingot. The tests were conducted at temperatures of -40 °C, -20 °C, 0 °C, +20 °C after conditioning for 15 minutes in a mixture of liquid nitrogen and isopropanol. Temperature measurements were performed using a Center 309 digital thermometer. The time of placing samples in the testing device was less than 5 seconds. The measurement results were averaged, and confidence intervals and standard deviation were determined according to the t-Student distribution. Test series consisted of a minimum of 3 samples for all considered combinations of heat treatment parameters.

The CCT diagram and the mechanical property test results for chromium- and titanium-alloyed cast steel were compared to corresponding data obtained for a reference cast steel, which underwent the same technological treatments, had a similar carbon content, and lacked alloying elements. This comparison facilitated the assessment of the effects of chromium and titanium on selected mechanical properties and the transformations occurring during continuous cooling.

3. Results and discussion

3.1. Material characterization (microstructural analysis)

The microstructure of cast steel alloyed with chromium and titanium directly after casting consisted of quasi-pearlite and ferrite, which was located both at the grain boundaries of former austenite and inside the grains (Fig. 1a). Ferrite areas, mainly allotromorphic, constituted a smaller portion of the microstructure than would be expected from the carbon content, indicating significant undercooling

and the action of alloying additions. The microstructure analysis conducted using a scanning electron microscope revealed details of the cementite laths' structure (Fig. 1b). Individual grains were characterized by varied dispersion, and the average distance between the laths was 0.28±0.17 μm. Additionally, features of the morphology of individual laths such as varied length and shape (there were also precipitations of a shape close to spheroidal), cracks, uneven distribution, or variable directionality were observed. Furthermore, bridges as well as local precipitations of cementite in the form of a network located at the grain boundaries of former austenite were noticed. The network was not smooth and contained certain protrusions, giving rise to new laths. Such varied morphology can affect crack resistance and the strength of the material. Areas with varied dispersion of laths may show variable resistance to dynamic loads, and the presence of bridges can affect the way stresses are transferred. At the grain boundaries of former austenite, there were also fine spherical cementite precipitations from which the growth of individual laths also occurred.

The microstructure of alloyed cast steel in the hardened state exhibited a lath morphology with a small proportion of components characterized by a needle-like structure (Fig. 2a). The application of electron microscopy techniques, both scanning (Fig. 2b) and transmission (Figs. 3a and 3b), revealed that a significant component of the microstructure was lower bainite, and to a lesser extent, quenching martensite. The structure of bainite was typical, consisting of ferritic laths and carbides oriented at 60° to their axis. It should be mentioned that the ferrite laths showed varied sizes. Such a complex microstructure may be desirable due to the possible higher strength properties. Research on 102Cr6 steel, which was subject to heat treatment aimed at achieving 20% lower bainite in the microstructure, allowed for obtaining higher strength properties than in the case of a microstructure composed solely of martensite [32]. This was due to the diffusion of carbon into the austenite rejected by the forming bainite, which increased the strength of the subsequently formed martensite. In the case of the analyzed material, this effect may be lesser due to the relatively small proportion of the martensitic phase in the microstructure. Tempering at 200 °C led to a reduction in the degree of carbon supersaturation of the ferritic phase and an increase in the share of fine carbide precipitations (Figs. 4a and 4b). Furthermore, a clear hierarchical structure was maintained. During the cooling of low- and medium-carbon steels, there is a division of the austenite grain into packets along habit planes, which create high-angle boundaries [33]. Packets are built from blocks of approximate crystallographic orientation (low-angle boundaries), which in turn are composed of laths, constituting the crystallographic cell of martensite. According to the Kurdjumov-Sachs theory, 24 variants of crystallographic orientation of laths are possible [34], because during the shearing process, one of the six {110} slip planes of martensite aligns parallel to one of the four {111} slip planes of austenite [33, 35]. According to available studies, it is believed that the size of both packets and blocks contributes to increasing strength properties and crack resistance [33, 36, 37]. Similar conclusions were also formulated in works [33, 38], where it was shown that packet boundaries can constitute a strong obstacle to the movement of dislocations, and the refinement of the microstructure increases the conventional yield limit. The microstructure after tempering at 400 °C was typical for steels tempered in this temperature range and consisted of acicular ferrite and numerous fine carbides (Fig. 5a and 5b). However, metallographic studies after tempering at 600 °C showed that the microstructure was composed of ferrite, in which local recrystallization occurred, and coagulated carbide precipitations (Fig. 6a and 6b). Therefore, two characteristic areas could be distinguished, the first where the phase deformation of ferrite was

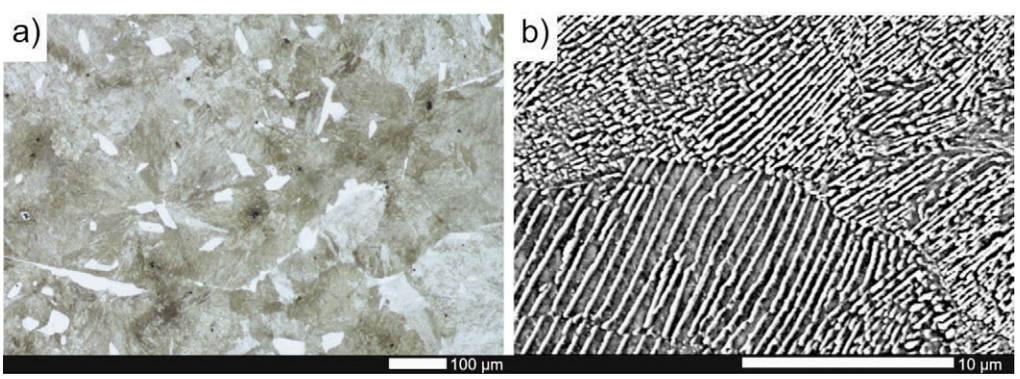

Figure 1. *Microstructure of cast steel with Cr and Ti in the raw state: a) LM; b) SEM. Etched with 3% HNO_3*

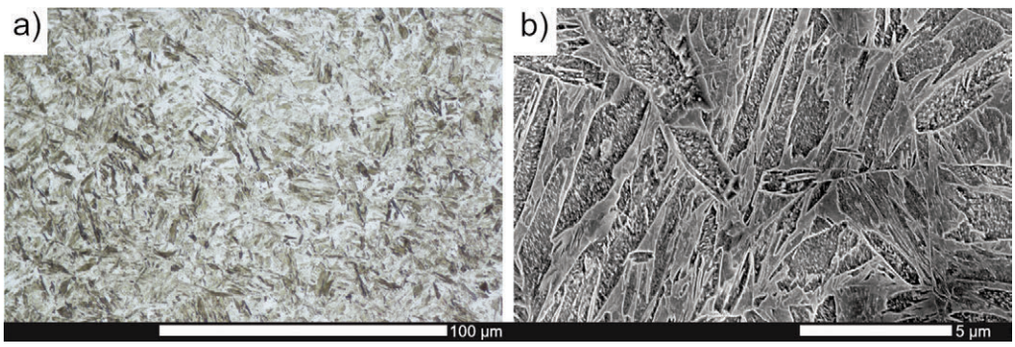

Figure 2. *Microstructure of cast steel with Cr and Ti after quenching: a) LM; b) SEM. Etched with 3% HNO_3*

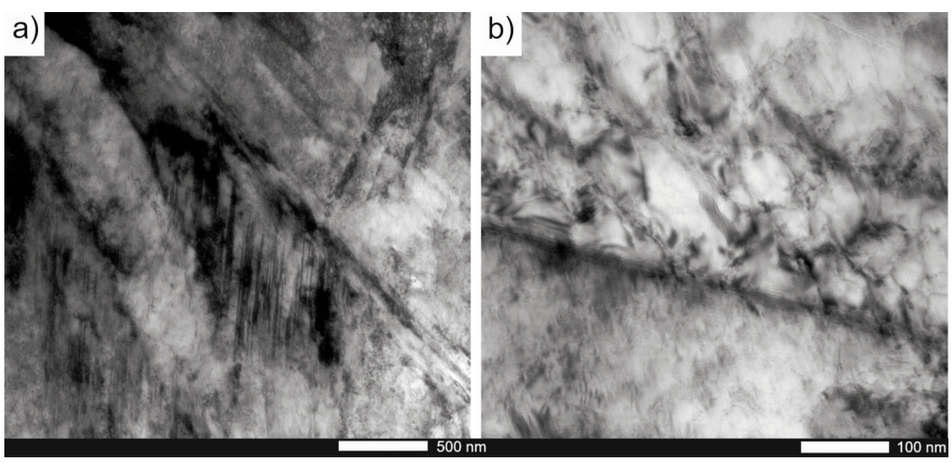

Figure 3. *Bainitic microstructure of cast steel with Cr and Ti after quenching: a) dark field, b) dark field. Etched, TEM*

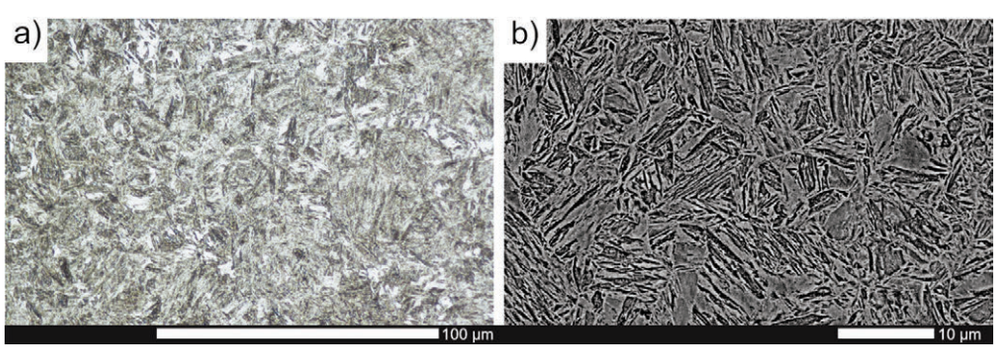

Figure 4. *Microstructure of cast steel with Cr and Ti after quenching and tempering at 200 °C: a) LM, b) SEM. Etched with 3% HNO_3*

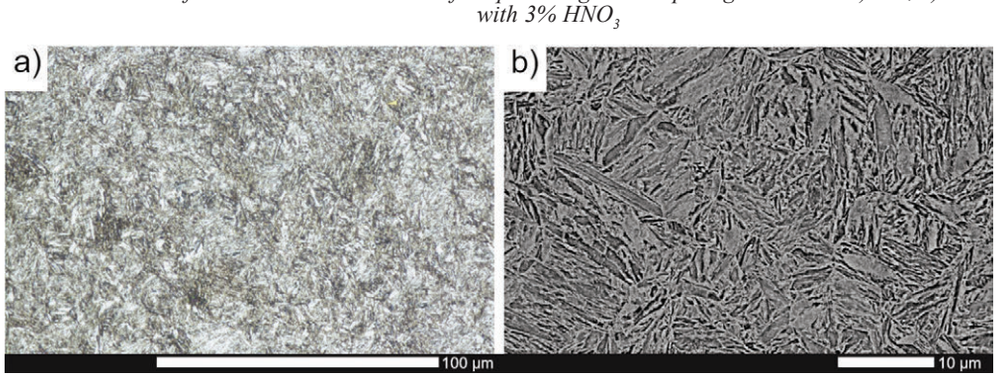

Figure 5. *Microstructure of cast steel with Cr and Ti after quenching and tempering at 400 °C: a) LM, b) SEM. Etched with 3% HNO_3*

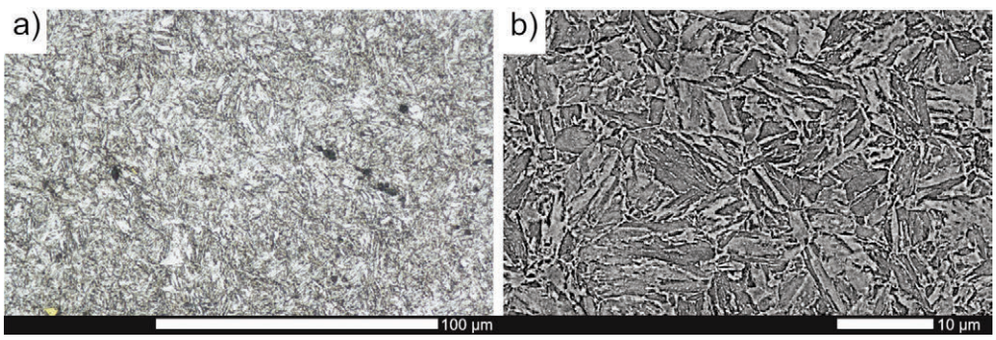

Figure 6. *Microstructure of cast steel with Cr and Ti after quenching and tempering at 600 °C: a) LM, b) SEM. Etched with 3% HNO_3*

maintained, and the second, where the ferrite underwent recrystallization. In the presented microstructure images, large regular precipitations of titanium nitrides in the form of regular polygons with yellow-orange coloring were visible.

3.2. Effect of chromium and titanium on phase transformation during continuous cooling

The CCT diagram for chromium and titanium alloyed cast steel is presented in Figure 7. To illustrate the impact of alloying elements on the transformations occurring during continuous cooling, Figure 7 also includes the CCT diagram for a reference cast steel that does not contain these elements.

In the case of the alloyed cast steel, the martensite start (M_s) temperature was 310 °C, and the critical cooling rate was slightly greater than 10 °C/s (Fig. 7). Furthermore, the M_s' temperature resulting from segregation and carbide precipitation along the grain boundaries of former austenite was revealed. The precipitated carbides locally reduced the carbon concentration around the boundaries, and these areas were characterized by a higher starting temperature of the martensitic transformation. The open field of bainite was characteristic, and the bainitic transformation itself, shifted towards longer times, began along with the ferritic transformation. Therefore, upon cooling at least the critical rate, it is possible to obtain a microstructure composed solely of martensite with lath morphology, which is typical for low-carbon steels (Figs. 8a and 8b). However, obtaining a microstructure composed only of martensite and bainite is not possible. As the cooling rate decreased, ferrite appeared in the microstructure alongside bainite (Fig. 8c). From the perspective of the bainitic transformation itself, the lowest possible start temperature of this transformation (B_s) is crucial, as there is a risk of unfavorable upper bainite appearing in the microstructure, which causes a decrease in toughness. With the decrease in cooling rate, the B_s temperature underwent only minor changes, reaching a value of 500 °C. Based on the analysis of the obtained microstructures, it can be stated that upper bainite in the analyzed melt was present only in the sample cooled at a rate of 1 °C/s (Fig. 8e). Interestingly, the ferrite field is separated from the bainitic transformation field by the austenite field. Slightly after the ferritic and bainitic transformations began the pearlitic transformation, and the sample cooled at a rate of 5 °C/s had a microstructure composed of ferrite, pearlite, upper and lower bainite, and martensite (Fig. 8d). This state was also maintained after slower cooling at 1 °C/s and 0.5 °C/s. However, a microstructure most closely resembling the equilibrium microstructure, composed exclusively of ferrite and pearlite, appeared only after cooling at a rate of 0.1 °C/s (Fig. 8g). Also noteworthy is the high hardness after cooling at a rate of 100 °C/s, amounting to 605HV5. Values significantly above 500 HV5 were also maintained in the case of samples cooled at rates of 10 °C/s and 50 °C/s.

Chromium is well-documented for its role in improving the hardenability of steel by shifting the continuous cooling transformation curves towards lower cooling rates, thereby promoting the formation of martensite. In addition to enhancing hardenability, titanium plays a crucial role in grain refinement and the formation of stable carbides, contributing to the overall stability of the microstructure. The combined presence of chromium and titanium in the alloyed cast steel resulted in a pronounced delay in phase transformations, with a notable increase in the retention of hard phases such as bainite and martensite across a broader spectrum of cooling rates. One critical observation was that the martensite start (M_s) temperature for the alloyed cast steel was approximately 80 °C lower than that of the reference cast steel. This indicates that the martensitic transformation in the alloyed material occurs at lower temperatures, allowing for the nucleation of martensite at reduced cooling rates. Despite this lower M_s temperature, the alloyed cast steel exhibited a

greater ability to retain martensite at slower cooling rates, significantly enhancing its hardenability. As a result, the alloyed cast steel was capable of achieving a fully martensitic microstructure even at cooling rates as low as 10 °C/s. In contrast, the reference cast steel, under similar cooling conditions, undergone partial phase transformations to ferrite and pearlite, which ultimately limit its hardness and mechanical properties. The presence of chromium and titanium not only delayed martensitic transformation but also significantly delayed bainitic and pearlitic transformations. This effect was particularly evident in the slower cooling regime, where the alloyed cast steel retained a predominantly martensitic microstructure, while the reference cast steel showed a greater propensity to transform into pearlite and bainite. The hardness measurements derived from the CCT diagrams further emphasize the disparity between the alloyed and reference cast steels. The alloyed cast steel exhibited significantly higher hardness values at faster cooling rates (around 100 °C/s), primarily due to the increased volume fractions of martensite and bainite. At slower cooling rates, the alloyed steel maintained hardness levels exceeding 300-400 HV, whereas the reference cast steel showed a substantial decrease in hardness, attributed to the formation of ferritic and pearlitic phases.

3.3. Effect of chromium and titanium on mechanical properties

The tensile test results (Fig. 9) indicate that in the as-cast state, the steel with chromium and titanium was characterized by a proof strength ($R_{p0.2}$) of 482 MPa, a hardness of 251 HBW, and unsatisfactory plastic properties, represented by elongation (A) and reduction of area (Z) after fracture, not exceeding 4%. This condition unequivocally points to the deterioration of plastic properties. After comprehensive heat treatment including quenching, there was an increase in strength indicators. In this state of heat treatment the steel was characterized by high strength properties, i.e. a hardness of 558 HBW (increase of 122%) and a yield strength of 1346 MPa (increase of 179%), while having low ductility, where the elongation after fracture was 3%, and the reduction of area after fracture was 1%. Such high strength properties, preceded by microstructural analysis and chemical composition, showed that the high strength properties result from two main strengthening mechanisms. They are realized by grain boundary strengthening through the refinement of austenite and significant supersaturation of ferrite with carbon, ensured by high hardenability. However, the low values of elongation and reduction of area define the analyzed material as not ductile under static load conditions. Very high strength properties of 512 HBW (104% increase relative to cast state) and 1331 MPa (176% increase relative to cast state) were maintained after additional heat treatment including low tempering, unfortunately, they still did not correspond with satisfactory plastic properties, represented by elongation and reduction of area after fracture, exceeding 7%. Tempering at 400 °C caused a decrease in yield strength and hardness compared to the previous state. The yield strength decreased to 1218 MPa, and hardness to 467 HBW. Simultaneously, it did not induce a satisfactory increase in parameters determining plastic properties, i.e., elongation and reduction of area, after fracture. In the quenched and tempered at 600 °C state, there was a clear improvement in the material's plasticity. The elongation and reduction of area after fracture were 14% and 18%, respectively. This condition was

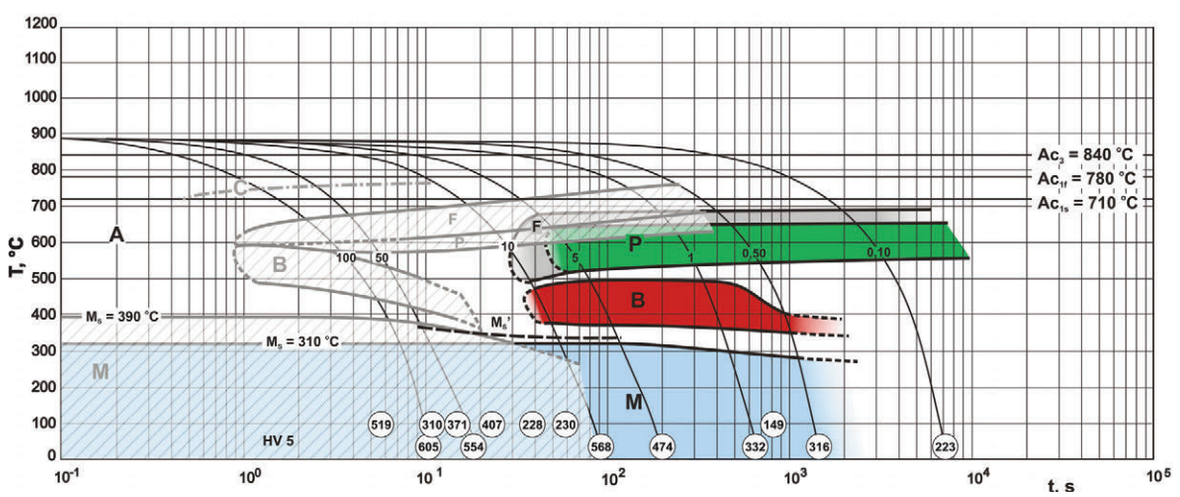

Figure 7. *CCT diagrams of the cast steel with Cr and Ti, and reference cast steel*

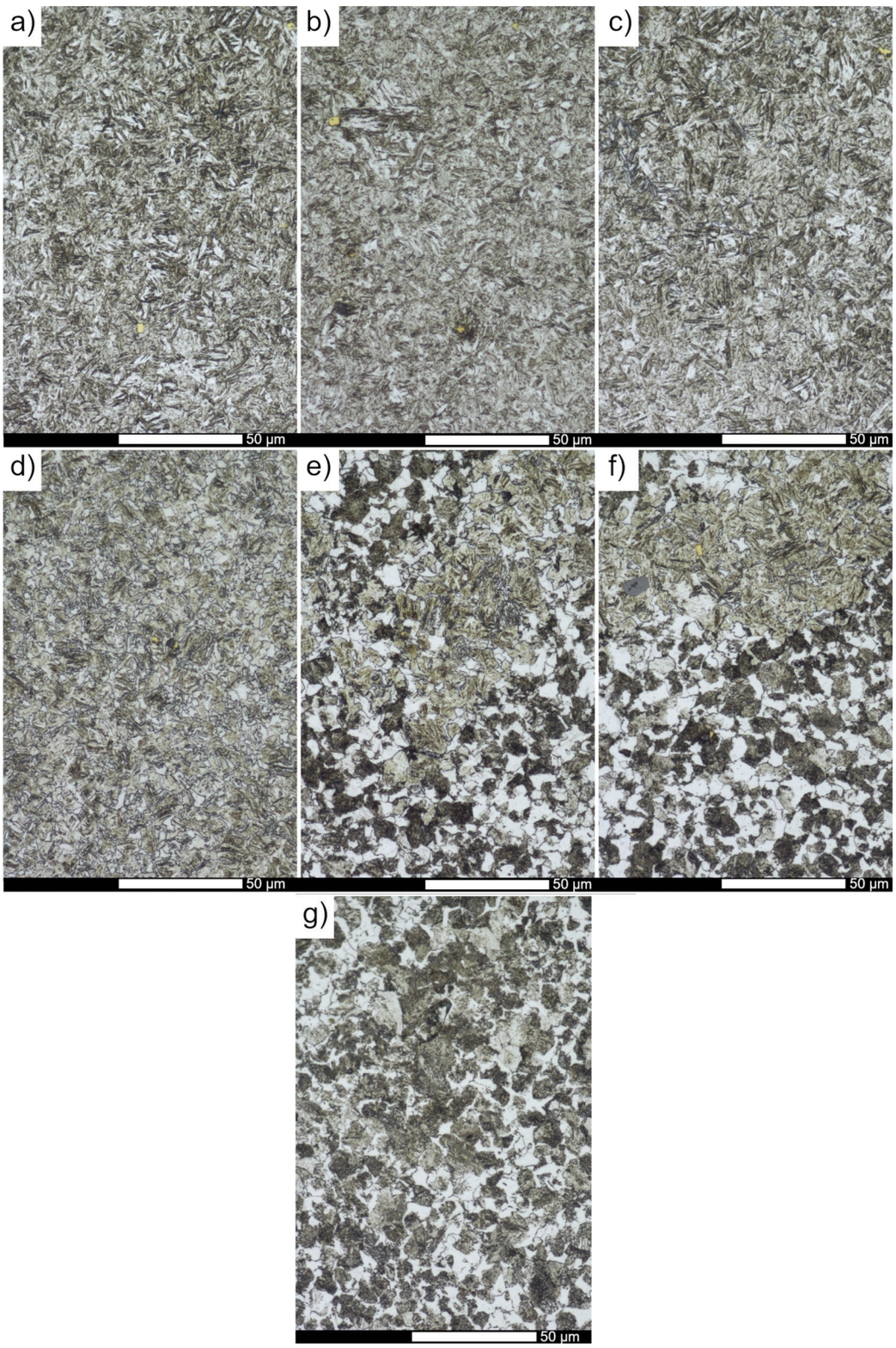

Figure 8. *Microstructure of cast steel with Cr and Ti obtained after cooling with different rates from temperature of 890 ºC: a) for cooling rate 100 °C/s, LM; b) for cooling rate 50 °C/s, LM; c) for cooling rate 10 °C/s, LM; d) for cooling rate 5 °C/s, LM; e) for cooling rate 1 °C/s, LM; f) for cooling 0.5 °C/s, LM; g) for cooling rate 0.1 °C/s, LM. Etched with 5% HNO_3*

maintained, with a successive reduction in hardness to 276 HBW and yield strength to 814 MPa. However, it is important to note the specific effect caused by this heat treatment. Although the microstructure's hardness was similar to the as-cast state, there was an increase in yield strength by over 75% compared to that material state.

In the state immediately after casting, the reference steel exhibited low hardness and yield strength, measured at 168 HBW and 290 MPa, respectively. Despite these lower values, the steel demonstrated high elongation and relative reduction of area after fracture, indicating that favorable plastic properties were maintained. Following quenching, the steel's hardness increased significantly to 589 HBW, with a corresponding rise in yield strength to 1075 MPa. However, the low values of the A and Z parameters clearly indicate that quenching led to a material state characteristic of brittleness. Tempering at a low temperature improved the ductility of the material, with the A parameter increasing to 8% and Z to 6%. This improvement in ductility occurred alongside a 13% decrease in hardness compared to the quenched state, while the yield strength remained unchanged. This behavior can be attributed to a balance between the reduced degree of solution hardening and the enhanced precipitation hardening due to the formation of finely dispersed carbides. A significant reduction in hardness and yield strength was observed only after tempering at 400 °C, where these values dropped to 380 HBW and 804 MPa, respectively. The relative elongation after fracture returned to levels similar to those in the as-cast state, while the Z parameter increased to 23%. After tempering at the highest temperature of 600 °C, the hardness further decreased to 226 HBW, and the yield strength dropped to 547 MPa. Notably, the A parameter increased by more than 40%, indicating a substantial recovery in ductility.

The hardness of the alloyed cast steel consistently surpassed that of the reference cast steel across nearly all heat treatment conditions. Upon quenching, both types of cast steel exhibited substantial increases in hardness. Notably, the alloyed cast steel maintained superior hardness values throughout the tempering process, suggesting enhanced resistance to tempering. The yield strength of the alloyed cast steel followed a similar trend to hardness, showing significant improvements over the reference cast steel. In its as-cast state, the alloyed steel exhibited superior yield strength, which was further augmented by quenching. Although yield strength decreased in both steels with increasing tempering temperatures, the alloyed cast steel consistently exhibited higher values.

In terms of ductility parameters, the reference cast steel generally exhibited higher values under most heat treatment conditions. This trend was particularly evident in the as-cast state, as well as after quenching and tempering at 400 °C. After tempering at the highest temperature, both percentage elongation and reduction in area after fracture were greater for the reference cast steel. Nevertheless, the ductility values for the alloyed cast steel remained satisfactory.

The results presented in Fig. 10 for the impact test vary depending on the heat treatment state and test temperature. In the as-cast state, the analyzed material with chromium and titanium was characterized by low impact toughness values of less than 5 J/cm^2, clearly indicating the occurrence of brittle cracking under dynamic loads. Quenching, preceded by heat treatment aimed at homogenizing the chemical composition and refining the microstructure, resulted in an increase in impact toughness to values above 16 J/cm^2 (at temperatures of +20 °C and 0 °C). However, at negative temperatures, the impact toughness was 12 J/cm^2 and 10 J/cm^2, respectively, for test temperatures of -20 °C and -40 °C. These values, although higher than those immediately after casting, also indicate the occurrence of brittle decohesion, especially considering the arbitrarily adopted threshold value of impact toughness of 35 J/cm^2, which serves as a criterion for brittleness corresponding to the occurrence of a 50% share between ductile and brittle fracture. This could lead to the phenomenon of brittle cracking in the analyzed steel, already evident at room temperatures. Conducting an additional tempering treatment at 200 °C led to a further increase in impact toughness. In this state of heat treatment, the material was characterized by an impact toughness of 20 J/cm^2 (at test temperatures of +20 °C and 0 °C), whereas at negative temperatures, the impact toughness dropped to 11 J/cm^2 (at -40 °C). Tempering at 400 °C did not result in the expected increase in impact toughness, which reached values similar (at room temperature) or even lower (at reduced temperatures) than in the quenched state, unequivocally indicating the occurrence of temper brittleness. Only the conducted heat improvement led to an increase in ductility, and only in this state of heat treatment did the impact toughness exceed the value of 35 J/cm^2, reaching 44 J/cm^2 (at room temperature). This state was not maintained at reduced temperatures, indicating that the transition from ductile to brittle state for the analyzed steel occurred already at positive temperatures. The relative difference between the highest and lowest impact toughness values was about 66%, with the lowest value obtained at a test temperature of -40 °C. These observations are consistent with the existing literature. Researchers often observe a decrease in tensile strength and impact

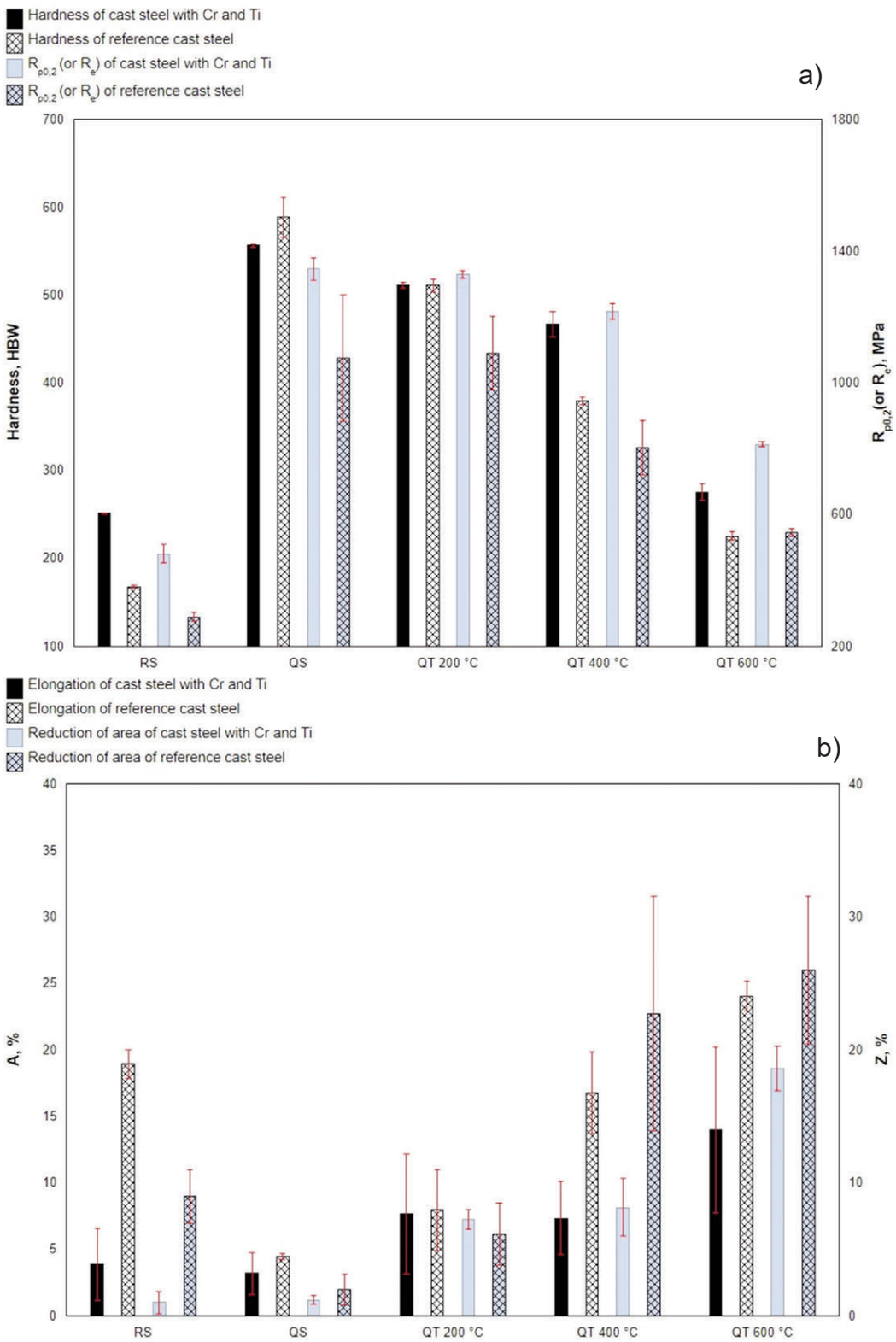

Figure 9. *Selected mechanical properties of the cast steel with Cr and Ti and the reference cast steel in different heat treatment states: a) hardness, yield point, b) percentage elongation, reduction of area after fraction. RS – raw state, QS – quenched state, QT 200 °C – quenched and tempered at 200 °C, QT 400 °C – quenched and tempered at 400 °C, QT 600 °C – quenched and tempered at 600 °C*

toughness due to the precipitation of coarsely dispersed TiN inclusions [26, 39], especially when their size exceeds 1 μm [18]. Crack propagation on titanium nitrides has been observed in both ferritic-pearlitic and bainitic steels [24].

In the as-cast state, the impact toughness of the reference cast steel ranged from 4 to 10 J/cm², only marginally higher than that of the alloyed steel. Hardening improved the material's impact toughness at reduced temperatures; however, the resulting values, ranging from 9 to 14 J/cm², remained lower than those of the chromium- and titanium-alloyed steel. Tempering at 200 °C following quenching led to a gradual increase in impact toughness across the entire temperature range tested, although the transition from ductile to brittle behavior occurred at temperatures near 0 °C. This heat treatment condition also exhibited significant variability in the results. In contrast, the quenched and tempered states at 400 °C and 600 °C displayed distinct properties. Under these conditions, the impact toughness values consistently exceeded the embrittlement criterion of 35 J/cm² across the entire temperature range, significantly surpassing those of the alloyed cast steel.

In impact toughness studies, a direct analysis of the nature of the fracture is crucial, as the previously described threshold criterion of 35 J/cm^2 does not always correspond to an even distribution between ductile and brittle fractures. Figures 11, 13, 14, 16 and 17 present macroscopic images of fractures in the analyzed steel with chromium and titanium after the impact test across the entire temperature range of the experiment, taking into account all states of heat treatment. Fractures in the as-cast state, in every instance, showed a lack of macroscopic deformation and practically no presence of ductile side zones and beneath the mechanical notch. The fracture surface was rough and did not exhibit complexity.

The detailed observations provided by the scanning electron microscope allowed for a thorough fractographic analysis in three typical locations: under the mechanical notch, in the central part of the sample, and on the side opposite to the mechanical notch. In the as-cast state, the morphology of the fracture zones was consistent across the entire temperature range of the test, as indicated in (Fig. 12). The nature of the material fracture immediately after casting was mixed – both transgranular and intergranular. The presence of intergranular cracks clearly points to brittle cracking. This aligns with information found in the literature [40], where intergranular fractures are typical for steels that have not undergone heat treatment. Despite the predominantly cleavage nature of the fracture, symptoms of very minor plastic deformations were also visible, especially at the boundaries of the crystallites and along lines described in the literature as "river" patterns [40]. Cracks from different grains converge at their boundaries. In some regions of the fracture surface, these lines radiate outwards, indicating their initiation from a point source [40]. The formation of characteristic steps indicates that the crack within a single grain proceeded along several parallel crystallographic planes, namely cleavage planes, characterized by causing the least plastic deformation as they progress [41]. As a result, visible steps formed, indicating that the crack lines changed crystallographic planes during propagation, overcoming the dividing layers of material through shearing or secondary cracking. Despite the brittleness of the material, "river" lines are accompanied by small plastic deformations at the fracture surface. Their presence, despite the significantly reduced temperature of the fracture test, results from the fact that some grains in the material are oriented unfavorably for the ongoing cracking, or are characterized by a stress state that does not favor it. The specific crystallographic orientation of a given grain may determine whether the crack will propagate over its surface in a brittle or ductile manner. The jumping of cracks across cleavage planes results from shearing or breaking of bridges, whose plastic crushing, along with the accumulation of stresses at the crack front, are the reasons for the appearance of plastic zones between the crystallites.

According to information available in the literature, steps (or offsets) occur when the crack front encounters an obstacle, such as a screw dislocation, and their size is related to the Burgers vector. The detection of traces of this phenomenon provides relative information about the amount of energy required for a fracture to occur – steps and the "river" patterns they create are observed when a larger amount of energy is absorbed, as the crack encounters an obstacle that prevents it from remaining on a single plane. Therefore, the formation of steps can be associated with a reduction in brittleness [40]. The steps were defined by Kocańda as an "index of crack arrest" [42]. Another piece of information they provide is the direction of crack propagation, which is approximately parallel to the edges of the steps [42]. The conducted microanalysis allowed for the identification of the widespread presence of the described steps in all states of heat treatment, as long as intergranular fracture areas appeared on them. This means that the type of heat treatment conducted was not a determining factor in the formation of steps in the brittle fracture areas that contribute to the absorption of cracking energy, though it depends on it for the size of the brittle fracture surface. Observation

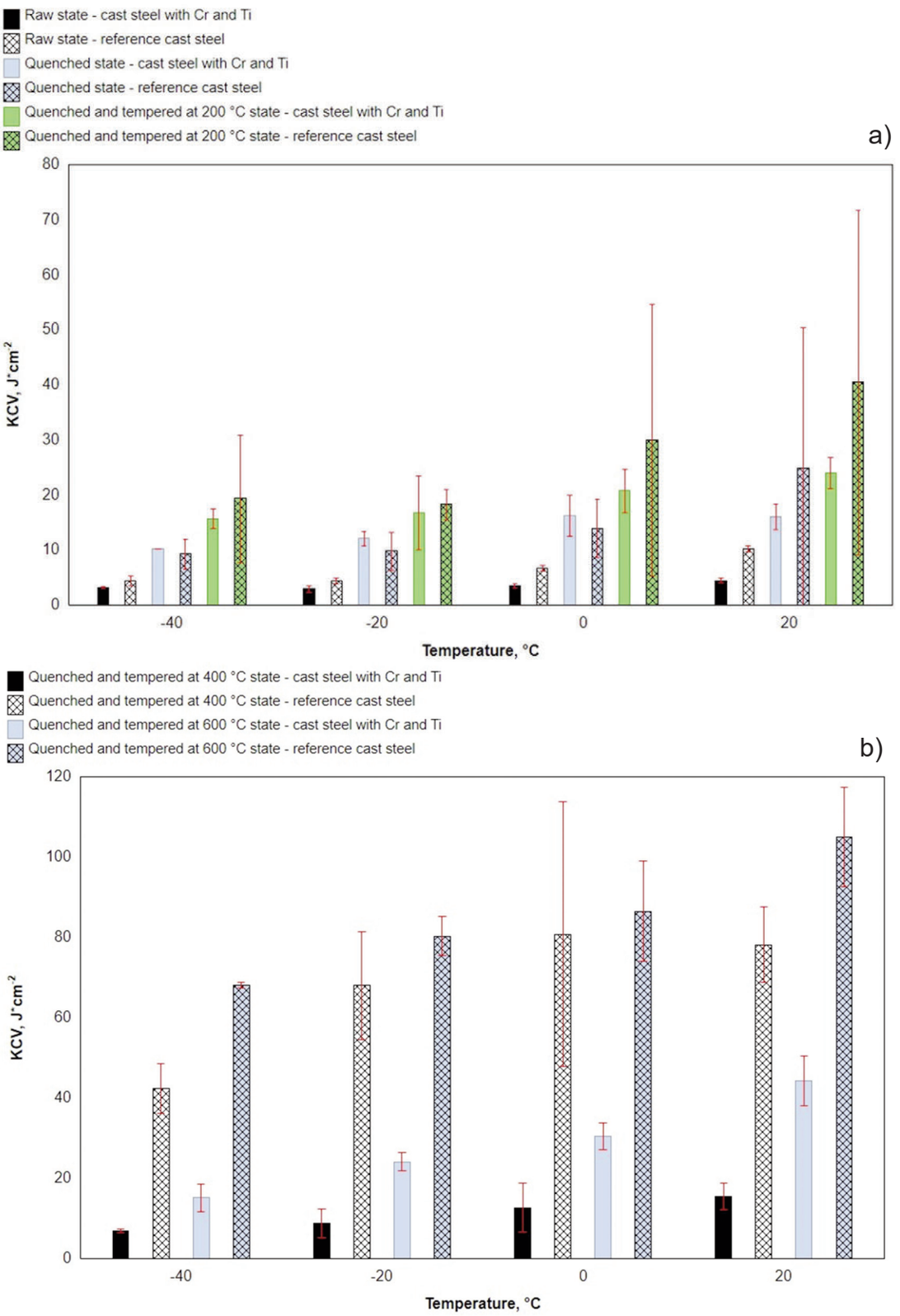

Figure 10. *Impact toughness as a function of temperature for cast steel with Cr and Ti and reference cast steel in different heat treatment states: a) raw state, quenched state, quenched and tempered at 200 °C, b) quenched and tempered at 400 °C, quenched and tempered at 600 °C*

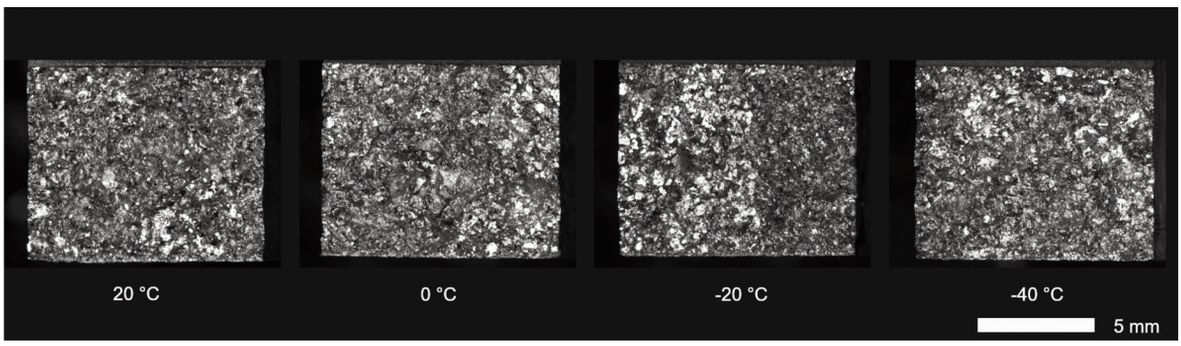

Figure 11. *Macroscopic image of fractures of cast steel with Cr and Ti in the as-cast condition, after impact testing at temperatures of 20 °C, 0 °C, -20 °C, and -40 °C. Unetched state, stereoscopic microscopy*

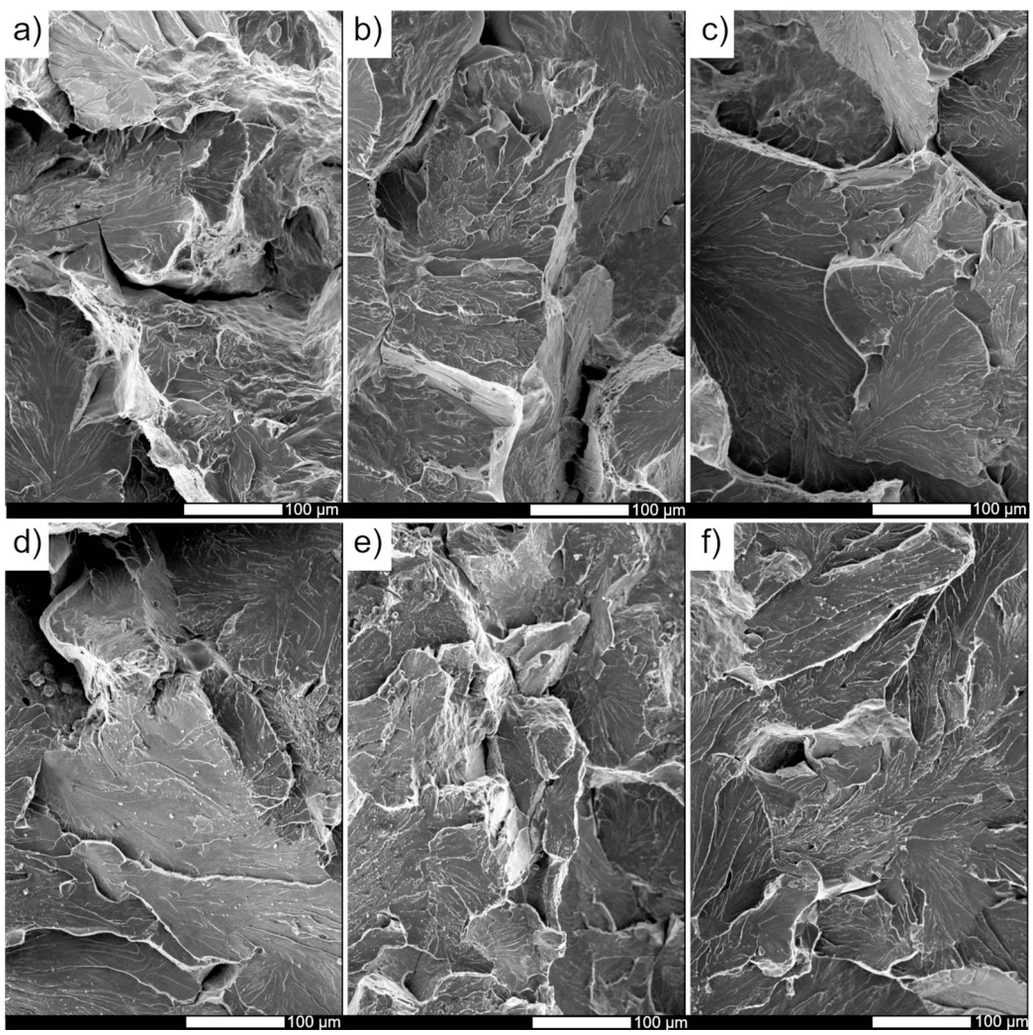

Figure 12. *Fracture zones of cast steel in the as-cast condition after impact testing at temperatures of 20 and -40 °C: a) zone under the notch at temperature 20 °C, b) central zone at temperature 20 °C, c) zone opposite to the notch at temperature 20 °C, d) zone under the notch at temperature -40 °C, e) central zone at temperature -40 °C, f) zone opposite to the notch at temperature -40 °C. Unetched state, SEM*

of steps can thus provide information on the movement of dislocations during deformation. The encounter of steps caused by dislocations of opposite signs can lead to the disappearance or reduction in the height of the larger step, whereas in the case of encounters of steps caused by dislocations of the same sign, it results in an increase in height [42]. The steps formed in the material reflect the grain size and

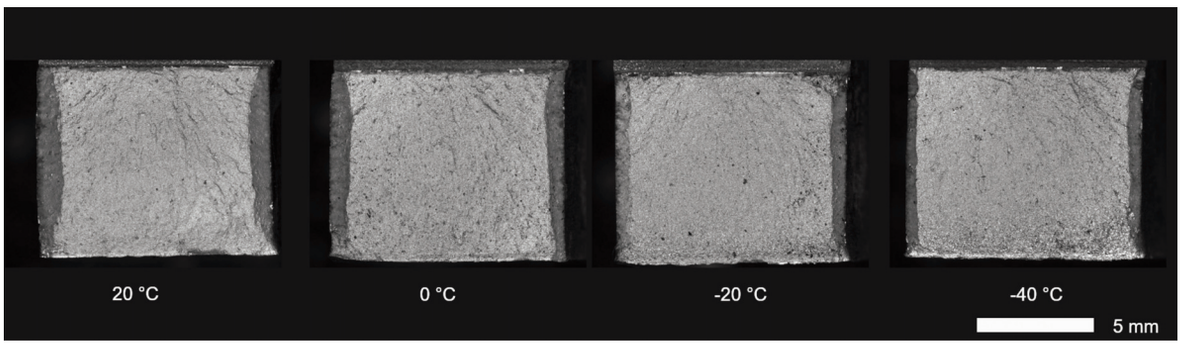

Figure 13. *Macroscopic image of fractures of cast steel with Cr and Ti in the quenched condition, after impact testing at temperatures of 20 °C, 0 °C, -20 °C, and -40 °C. Unetched state, stereoscopic microscopy*

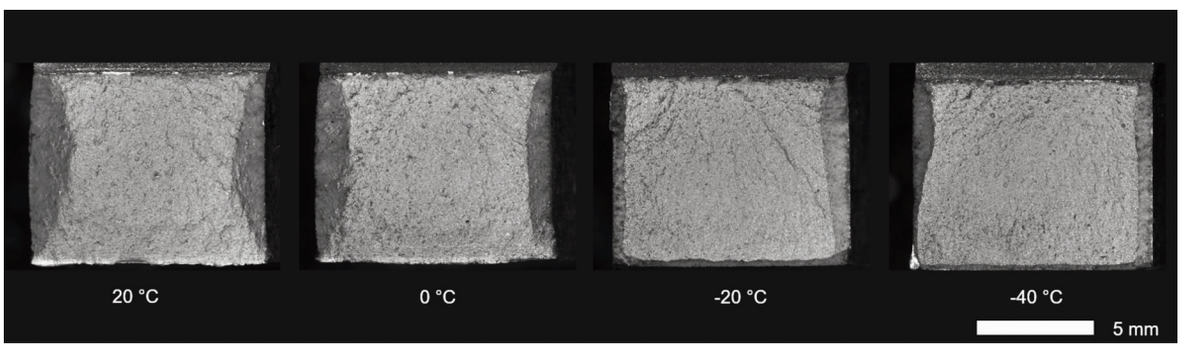

Figure 14. *Macroscopic image of cast steel with Cr and Ti in the quenched and tempered at 200 °C condition, after impact testing at temperatures of 20 °C, 0 °C, -20 °C, and -40 °C. Unetched state, stereoscopic microscopy*

indicate the presence of a coarse-grained microstructure in the as-cast state. Additionally, the steps are accompanied by transgranular cracks that also run along the grain boundaries.

In the hardened state, the proportion of plastic zones ranged from about 12% (impact test at -40 °C) to about 25% (impact test at +20 °C). The central surfaces were characterized by fine granularity, and their topography was not elaborate (Fig. 13). This condition resulted in reduced toughness across the entire range of test temperatures in this steel. Only after low tempering were traces of macroscopic plastic deformation and wide lateral plastic zones noticed, comprising from 15% (impact test at -40 °C) to 35% (impact test at +20 °C) (Fig. 14). Microscopic analysis revealed characteristic morphological features of fractures in the hardened and low-tempered state (Fig. 15). The fractures were of a mixed nature – quasi-cleavage and plastic. The shares of plastic zones were larger in the case of tempered samples. The formation of plastic fracture surfaces is facilitated by the uniformity and fine granularity of the microstructure [40]. Plastic areas were characterized by a typical dimpled structure, formed as a result of enlarging micropores or microcracks. The dimples varied in size and depth, and on the bottom of some, fragmented spheroidal precipitations were visible, which did not damage during cracking. Since the dimples were mostly uniform, the resulting fractures can be classified as normal fractures. Quasi-cleavage fracture is typical for steel with a martensitic microstructure, as well as bainitic, at temperatures below the ductile-to-brittle transition temperature. This type of fracture occurs through brittle cracking in small, local areas, and then their connection into a single fracture surface as a result of plastic deformation. Although the facets here are similar to cleavage facets due to the presence of “river” patterns, the identification of crystallographic planes is almost impossible. It also cannot be described as a typical quasi-cleavage fracture because the “river” system, meandering, creates dimples over a large surface that in construction may resemble a ductile fracture. The ridges of quasi-cleavage facets were characterized by an elaborate topography. In the figure 15f, a step is visible protruding above the fracture surface, with a marked plastic fracture with a dimpled structure on the side, which may also indicate the extraction of a column from the matrix. It creates the impression that columns bind the separated surfaces. In the case of material fracture in the hardened state, it is also possible to notice the occurrence of typically cleavage areas with cleavage steps within the grains. The fracture surface is characterized by an elaborate topography, with larger elevations and pits, and numerous transverse cracks were observed. The

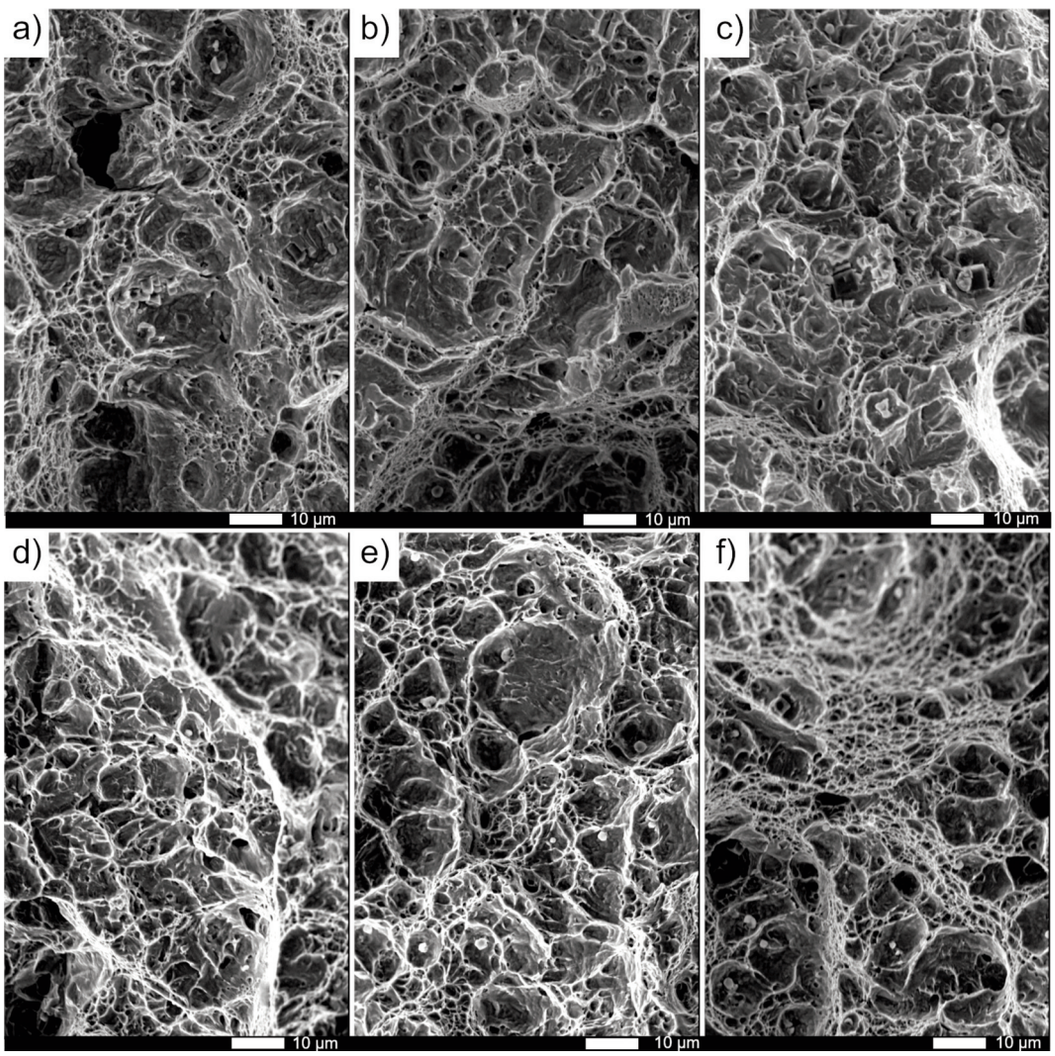

Figure 15. *Fracture zones of cast steel in the quenched condition and quenched and tempered at 200 °C: a) quenched condition, zone under the notch, temperature 20 °C, b) quenched condition, central zone, temperature 20 °C, c) quenched condition, zone opposite to the notch, temperature 20 °C, d) quenched and tempered at 200 °C, zone under the notch, temperature 20 °C, e) quenched and tempered at 200 °C, central zone, temperature 20 °C, f) quenched and tempered at 200 °C, zone opposite to the notch, temperature 20 °C. Unetched state, SEM*

presence of these areas, with a smaller proportion of plastic zones, resulted in lower impact toughness values compared to tempered samples. Cracks still created branches, but not as intensely as in the case of samples subjected to additional heat treatment. It is assumed that secondary cracks spread in the immediate vicinity of the main crack until they exhibit a characteristic discontinuity. One of the causes of these microcracks is the formation of microsteps on the fracture surface, which should be attributed to defects in the internal structure. In the case of crystalline bodies, these defects will be dislocations and grain boundaries [40]. As shown in the study [43], the dislocation density is higher in steel with finer grain.

In the tempered state at 400 °C, the proportion of plastic zones at each impact test temperature was lower than in the low-tempered state (Fig. 16). This confirmed the assumptions about the cause of lower toughness in this heat treatment condition. No traces of macroscopic deformation of the samples were noted either, and on the central surfaces, characterized by greater roughness, elevations radiating from the notch bottom were observed. Studies have shown [40] that transgranular cleavage cracks are initiated in areas where the highest stress concentration occurs, which is relatively close to the mechanical notch. A different fracture character was obtained after tempering at 600 °C (Fig. 17.). Most notably, macroscopic plastic deformation was observed, except for the fracture

obtained after the impact test conducted at the lowest temperature. The shares of plastic zones, mainly occupying areas at the side edges, ranged from 10% (at -40 °C) to 40% (at +20 °C). The central zones of fractures formed in the temperature range from +20 °C to -20 °C were characterized by an elaborate morphology showing the presence of pits. The developed fracture surface can result in high ductility confirmed by the results of the impact test, as a significant portion of the energy in the cracking process can be absorbed as surface energy in such cases.

The microscopic images obtained in three characteristic areas confirm the presence of a mixed fracture with complex features and morphology indicative of characteristic symptoms for both transgranular and intergranular cleavage fractures, while in the areas of cleavage ridges, a ductile fracture with a dimpled structure was observed (Fig. 18). The proportion of plastic areas was greater in the zone opposite the mechanical notch. The occurrence of a mixed fracture is characteristic of metals and alloys crystallizing in the A2 lattice, caused by the occurrence of plastic deformation in the initial phase, until the cold hardening induced creates conditions for cleavage cracking [40]. In the plastic areas, within the large-diameter dimples, spheroidal or cubic non-metallic inclusions were present. Cubic inclusions were titanium nitrides, which, being partially crushed, constituted local crack nucleation areas. The observed characteristics of the fractures indicate the need to consider the role of titanium nitride precipitations in the initiation, as well as the propagation of cracks. Literature research has shown that this topic has been addressed by numerous research teams. For example, Liu et al. [44] pointed out that in the cracking process initiated by TiN precipitations, three stages can be distinguished: initiation of microcracks on the nitride and their immediate reaching to the interfacial boundary of TiN-matrix without propagation into the matrix itself, then generation of new cracks, where many of them develop towards TiN, ultimately resulting in the separation of the nitride from the matrix, resulting in its chipping and the formation of a pit. It should also be kept in mind that both carbides and titanium nitrides are characterized by high hardness. The hardness of the analyzed precipitations in the cited work reached even 3200 HV, and higher hardness facilitates brittle cracking, especially under conditions of high stress. Meanwhile, Du [45], following previous research works [46, 47], believes that the formation of cleavage fractures initiated by titanium nitrides is accompanied by the following critical stages: nucleation of a microcrack on a TiN precipitation, then propagation of the microcrack through the TiN-matrix boundary, enveloping the entire grain with the crack, and finally spreading the crack beyond its boundary. The dominance of transgranular fracture results from the precipitations at grain boundaries of fine-dispersed carbides formed during the tempering process. The presence of non-metallic inclusions and carbides thus became the main factor conditioning transgranular cracking. Hard large precipitations, such as undoubtedly nitrides, undergo cracking, and when such cracking reaches a critical size, fulfilling the Griffith criterion, it can influence the increase in material brittleness. Cracking may also occur on carbide precipitations, leading to the formation of microcracks of critical size. Therefore, from the observation of precipitations, it can be inferred that the fracture occurred both along the precipitation-matrix boundary, indicating a typical intergranular course, and through the precipitations, i.e., transgranularly. This suggests a mixed nature of cracking, with intergranular fracture accompanied by areas of transgranular fracture. Microcrack initiation can occur at the tip of an inclusion or the place between two adjacent inclusions. In the case of crack initiation at the tips of inclusions, when the stress concentration reaches a critical value in the field of high stresses, in the case of fine-grained microstructure, there will be a large number of grains with high-angle boundaries and the crack will start to propagate into the matrix. However, dislocations and cracks have a high resistance, which, combined with the coordinated deformation of the nearby low-stress field microstructure, hinders the further development of cleavage cracks. In such cases, due to the fulfillment of the crack size criterion, in the case of microstructures characterized by fine granularity, cleavage or quasi-cleavage does not occur, which can be attributed to the large contact surface of fine grains with high-angle boundaries, which easily adapt to deformations, thereby reducing the stress concentration in the field of high stresses. Therefore, even if a microcrack is initiated by a titanium nitride, whether it penetrates into the matrix or not, depends on the level of stress (whether it exceeds the strength of the particle-matrix interface or not). Additionally, besides plastic zones, the cleavage ridges were places of characteristic steps forming a “river” pattern with relatively small branches. The interaction of grain boundaries on the cracking mechanism is undoubtedly a complex phenomenon, largely dependent on the precipitations containing foreign atoms present on them. The influence is not only due to the physicochemical properties of these phases but also their distribution and size. Under dynamic load conditions, as indicated by Maciejny [40], it is the phase precipitations at grain boundaries that can be attributed to the formation of this type of fracture. Comparing the obtained microstructural images, it can be concluded that the size of the facets corresponds to the size of ferritic blocks.

Microscopic analysis of the fracture structure in the tempered at 600 °C state indicates the occurrence of a mixed fracture, mainly proceeding intergranularly. Additionally, cleavage fracture surfaces were visible along the cleavage boundaries. The facets were larger than in the state tempered at 400 °C, reflecting the size of recrystallized grains or blocks in those areas that were not subject to the recrystallization process occurring at 600 °C. There were also cubic (titanium nitrides) inclusions, which essentially did not contain traces of damage, indicating that cracking occurred along the precipitate-matrix boundaries. Another detail of the discussed fracture was the presence of spheroidal carbide precipitations, present in plastic sections. This image could result from two processes related to the carbides being pulled out of the matrix or cracking proceeding along the carbide-ferrite boundary. Special cases of cleavage cracking along carbides are also known [42]. The facets were smooth, without the presence of steps, but regular cubic indentations could be distinguished, being traces of the presence of titanium nitrides. Additionally, transgranular cracks were highlighted at the boundaries. Cleavage areas were surrounded by fragments of ductile fracture sections forming filaments and covered with traces of inclusions forming a kind of microbubbles. Transitions between brittle and ductile microzones were quite abrupt. In the zone opposite the mechanical notch, the ductile fracture with a mixed structure dominated, consisting of a set of parabolic and regular dimples of varied diameters, as well as filaments. Larger dimples contained spheroidal mechanical inclusions. The obtained fracture had an unusual structure for heat-treated steels. This type of decohesion caused an adverse phenomenon of increasing the brittleness threshold in this heat treatment state and was associated with the presence of titanium nitrides, which, by blocking the migration of high-angle grain boundaries related to recrystallization processes, became crack initiation sites. This indicates a certain weakness of the interphase boundaries between titanium nitrides and ferrite. Du [45] observed, inhibition of crack propagation initiated on titanium nitrides in the case of fine-grained microstructure. When steel contained coarse-grained TiN particles, they were observed to be initiation sites for cleavage cracks when the average ferrite grain size ranged from 9.5-27.3 μm, however, in the case of a microstructure characterized by an average grain size of 5.0 μm, cleavage initiated by TiN was not observed. Therefore, grain size is key in the process of brittle cracking induced by TiN particles.

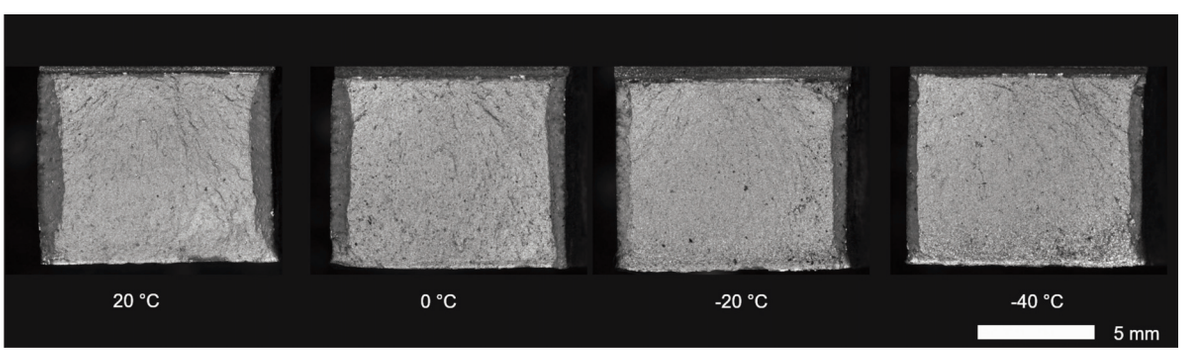

Figure 16. *Macroscopic image of fractures of cast steel with Cr and Ti in the quenched and tempered at 400 °C condition, after impact testing at temperatures of 20 °C, 0 °C, -20 °C, and -40 °C. Unetched state, stereoscopic microscopy*

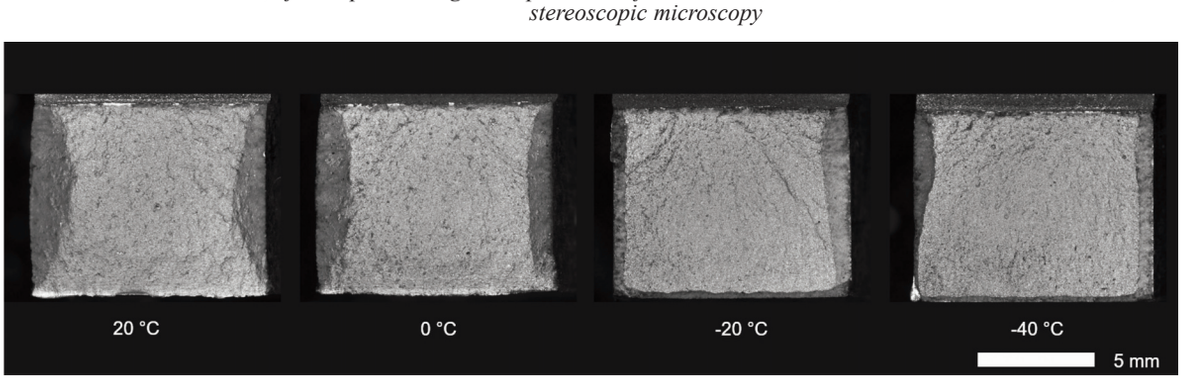

Figure 17. *Macroscopic image of fractures of cast steel with Cr and Ti in the quenched and tempered at 600 °C condition, after impact testing at temperatures of 20 °C, 0 °C, -20 °C, and -40 °C. Unetched state, stereoscopic microscopy*

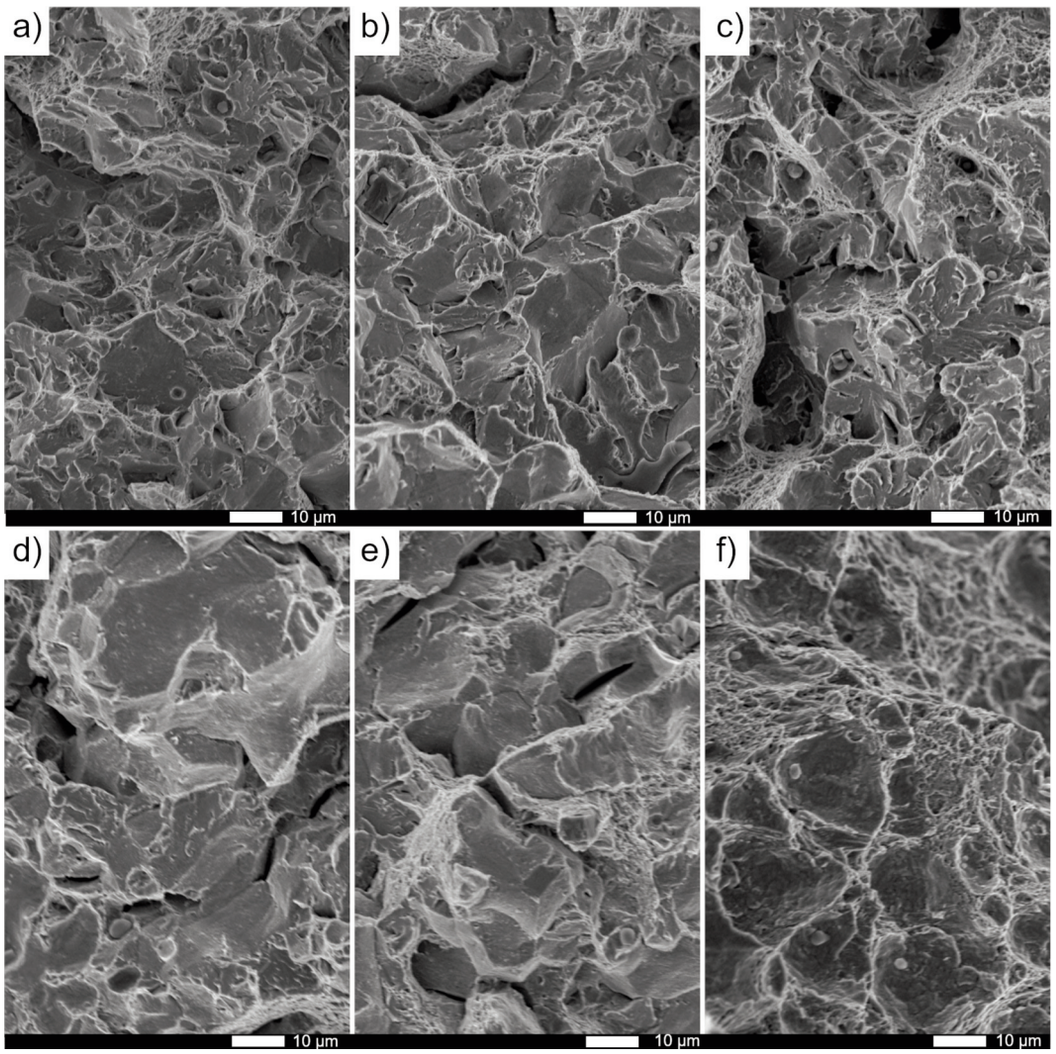

Figure 18. *Fracture zones of cast steel in the quenched and tempered at 400 and 600 °C condition: a) quenched and tempered at 400 °C, zone under the notch, temperature 20 °C, b) quenched and tempered at 400 °C, central zone, temperature 20 °C, c) quenched and tempered at 400 °C, zone opposite to the notch, temperature 20 °C, d) quenched and tempered at 600 °C, zone under the notch, temperature 20 °C, e) quenched and tempered at 600 °C, central zone, temperature 20 °C, f) quenched and tempered at 600 °C, zone opposite to the notch, temperature 20 °C. Unetched state, SEM*

4. Conclusions

The aim of this study was to analyze the influence of chromium and titanium on the microstructural and mechanical properties of medium carbon steel. In addition to the general objective of the study, the practical aspects of improving selected strength parameters based on conventional – commercially available in the industry – comprehensive heat treatment processes were also investigated. The conducted research has demonstrated that alloying additions such as chromium and titanium in medium-carbon steel make it possible to achieve a cast material characterized by high mechanical properties. It is important to emphasize that, in addition to the technological treatments, the achievement of the set objective required the implementation of a multifaceted research procedure that included microstructural, chemical, and strength tests, impact resistance studies, and comprehensive fractographic analysis. The topics covered can be characterized as follows:

1) Microstructural analysis of cast steel with chromium and titanium has shown that different heat treatment conditions result in microstructures with different morphologies, which are reflected in different values for all strength and impact indicators. After quenching, a significant presence of lower bainite was found in the microstructure, the details of

which were visualized using transmission electron microscopy.

2) The addition of chromium and titanium effectively stabilized the austenitic phase and delayed pearlitic and bainitic transformations. This resulted in increased hardenability and the retention of martensite at lower cooling rates. The higher hardness of the alloyed cast steel, especially around 605 HV at medium and high cooling rates, confirms that the presence of chromium and titanium significantly improves the mechanical properties.

3) The presence of chromium and titanium in the cast steel resulted in a significant improvement in hardness and yield strength, especially under tempering conditions. However, the alloyed steel in the quenched condition exhibited lower hardness than the reference steel, indicating a complex interaction between the alloying elements and the heat treatment processes. Nevertheless, the overall better performance of the chromium and titanium alloyed steel under most conditions showed that these elements effectively increase the strength of the cast steel.

4) From a ductility perspective, the average elongation, reduction in fracture surface area, and impact toughness observed in the as-cast condition and after quenching and tempering at low temperature, clearly indicate the presence of a brittleness threshold, even at room temperature. Tempering at 400 °C did not lead to the expected improvement in toughness of the alloyed cast steel. Instead, the toughness values both at room temperature and at reduced temperatures were comparable to or even lower than those in the quenched condition, indicating the presence of temper brittleness. However, subsequent heat treatments resulted in improved ductility, with impact toughness exceeding 35 J/cm² and reaching 44 J/cm² at room temperature. The simultaneous addition of chromium and titanium therefore led to a significant reduction in the plastic properties while the same time improving the resistance of the cast steel to tempering processes.

The fractographic analysis of cast steel with chromium and titanium showed detailed characteristics of the fracture structure in different heat treatment conditions. It was found that a transgranular cleavage fracture predominates in the state directly after casting. In the states with quenching and low tempering, mixed fractures with a predominance of transgranular quasi-split fractures were obtained. In the tempered condition at 400 °C, the proportion of plastic zones at each impact test temperature was lower than in the low tempered condition, while microscopic analysis confirmed the presence of a mixed fracture with complex features and a morphology indicating the presence of characteristic symptoms of both transgranular and intergranular cleavage fractures, with ductile fractures with dimple structure observed in the areas of the cleavage ridges. In the thermally enhanced condition, the fracture was characterized by an unusual structure for this heat treatment condition. The facets were smooth, without steps, but regular cubic indentations could be detected as traces of the presence of titanium nitrides. Moreover, transgranular cracks were visible at the edges. The cracked areas were surrounded by fragments of ductile fracture sections consisting of very fine dimples.

5) The study confirms that although chromium and titanium significantly improve the strength of medium carbon cast steel, these benefits come at the expense of reduced ductility and impact toughness, especially in the quenched and tempered at low temperature condition. The simultaneous addition of these elements requires careful consideration of their effects on microstructure and mechanical properties, particularly in applications where toughness is critical. Future work should explore alternative heat treatment strategies or alloy combinations to mitigate the brittleness associated with TiN precipitates while retaining the strength benefits of chromium and titanium.

6) It must be borne in mind that the choice of suitable material solutions depends on many factors, including not only technical aspects but also environmental and economic considerations. Modern trends assume ever-increasing performance of machines and equipment, which entails an intensification of wear processes and their negative impact on the environment. These trends are particularly evident in countries where a relatively large amount of minerals is extracted from open-cast mines. Consequently, there is a very high demand for new technical materials. The laboratory tests carried out add to the knowledge of cast steel materials and fit into the trend of searching for materials that meet the environmental requirements of open-pit mines. They thus become a starting point for research into technological and operational properties. It should also be emphasized that these significant environmental impacts, which determine the service life of machinery and equipment, can be somewhat limited thanks to the solutions offered by the modern metallurgical industry. With increasing consumption, global energy demand, fast transportation, and extensive road networks, open pit mines will not disappear from the landscape anytime soon. However, through the use of modern, high-strength materials, including casting materials, the mining industry can have a less destructive impact on the environment,

particularly by reducing emissions of harmful greenhouse gasses from equipment and working machinery.

Competing interest

On behalf of all authors, the corresponding author states that there is no conflict of interest.

Author Contributions

B.B: Writing – original draft, Visualization, Supervision, Project administration, Methodology, Formal analysis, Data curation. R.J.: Review & editing, Supervision, Methodology, Formal analysis. R.D.: Review & editing, Supervision, Methodology, Formal analysis. P.B.: Review & editing, Supervision, Methodology, Formal analysis. All authors have read and agreed to the published version of the manuscript.

Data availability

Data will be made available on request.

References

[1] L.A. Dobrzański, Metallic engineering materials, Publishing House "WNT", Warsaw, 2009.

[2] B. Kalandyk, Wear-resistant cast steel, in: Foundry Handbook. Volume 1. Materials (J.J. Sobczak Editor), Publishing House of the Technical Association of Polish Foundrymen, Krakow, 2013, p. 335–340.

[3] N. Yüksel, S. Şahin, Wear behavior - hardness - microstructure relation of Fe-Cr-C and Fe-Cr-C-B based hardfacing alloys, Materials & Design 58 (2014) 491–498. https://doi.org/10.1016/j.matdes.2014.02.032

[4] S.G. Sapate, A. Selokar, N. Garg, Experimental investigation of hardfaced martensitic steel under slurry abrasion conditions, Materials & Design 31 (2010) 4001–4006. https://doi.org/10.1016/j.matdes.2010.03.009

[5] J.H. Kim, K.H. Ko, S.D. Noh, G.G. Kim, S.J. Kim, The effect of boron on the abrasive wear behavior of austenitic Fe-based hardfacing alloys, Wear 267 (2009) 1415–1419. https://doi.org/10.1016/j.wear.2009.03.017

[6] P.B. Pawar, A.A. Utpat, Effect of chromium on mechanical properties of A487 stainless steel alloy, International Journal of Advance Research in Science and Engineering 5 (2016) 112–118.

[7] X. Chen, J. Liang, D. Yang, Z. Hu, X. Xu, X. Gu, G. Xie, Effect of chromium on microstructure and mechanical properties of hot-dip galvanized dual-phase (DP980) steel, Crystals 13 (2023) 1287. https://doi.org/10.3390/cryst13081287

[8] H. Jirková, L. Kučerová, B. Mašek, The Effect of Chromium on Microstructure Development During Q-P Process, Materials Today: Proceedings 2 (2015) S627–S630. https://doi.org/10.1016/j.matpr.2015.07.362

[9] R. Dąbrowski, J. Pacyna, Effect of chromium on the early stage of tempering of hypereutectoid steels, Archives of Metallurgy and Materials 53(4) (2008) 1017–1023.

[10] V.N. Zikeev, R.K. Guseinov, Effect of chromium on the properties of high-strength steel 30N9K4MF, Metal Science and Heat Treatment 21 (1979) 383–386. https://doi.org/10.1007/BF00780783

[11] T. Lin, Y. Guo, Z. Wang, H. Shao, H. Lu, F. Li, X. He, Effects of chromium and carbon content on microstructure and properties of TiC-steel composites, International Journal of Refractory Metals and Hard Materials 72 (2018) 228–235. https://doi.org/10.1016/j.ijrmhm.2017.12.037

[12] F. Han, B. Hwang, D.W. Suh, Z. Wang, D.L. Lee, S.-J. Kim, Effect of molybdenum and chromium on hardenability of low-carbon boron-added steels, Metals and Materials International 14 (2008) 667–672. https://doi.org/10.3365/met.mat.2008.12.667

[13] Y. Tian, J. Ju, H. Fu, S. Ma, J. Lin, Y. Lei, Effect of chromium content on microstructure, hardness, and wear resistance of as-cast Fe-Cr-B alloy, Journal of Materials Engineering and Performance 28 (2019) 6428–6437. https://doi.org/10.1007/s11665-019-04369-5

[14] H. Fu, J. Kuang, L. Wang, Microstructure, mechanical properties, and abrasive wear behaviour of Si-Mn-Cr-B cast steel as a function of carbon concentration, Steel Research International 79 (2008) 721–728. https://doi.org/10.1002/srin.200806190

[15] T.M. Scoonover, H.L. Arnson, Hardenability of low- and medium-carbon Mn-Cr-Ni-Mo steels, Journal of Heat Treating 3 (1984) 183–192. https://doi.org/10.1007/BF02833260

[16] I. El-Mahallawi, R. Abdel-Karim, A. Naguib, Evaluation of effect of chromium on wear performance of high manganese steel, Materials Science and Technology 17 (2001) 1385–1390. https://doi.org/10.1179/026708301101509340

[17] B. Loberg, A. Nordgren, J. Strid, K.E. Easterling, The role of alloy composition on the stability of nitrides in Ti-microalloyed steels during weld thermal cycles, Metallurgical Transactions A: Physical Metallurgy and Materials Science 15A (1984) 33–41. https://doi.org/10.1007/BF02644385

[18] Y. Zhu, Y.-M. Lu, C.-W. Huang, Y.-L. Liang, The effect of TiN inclusions on the fracture mechanism of 20CrMnTi steel with lath martensite, Materials Research Express 7 (2020). https://doi.org/10.1088/2053-1591/ab7ac3

[19] L.P. Zhang, C.L. Davis, M. Strangwood, Dependency of fracture toughness on the inhomogeneity of coarse TiN particle distribution in a low alloy steel, Metallurgical and Materials Transactions A 32 (2001) 1147–1155. https://doi.org/10.1007/s11661-001-0125-7

[20] O. Comineli, R. Abushosha, B. Mintz, Influence of titanium and nitrogen on hot ductility of C-Mn-Nb-Al steels, Materials Science and Technology 15 (1999) 1058–1068. https://doi.org/10.1179/026708399101506788

[21] B. Mintz, S. Yue, J.J. Jonas, Hot ductility of steels and its relationship to the problem of transverse cracking during continuous casting, International Materials Reviews 36 (1991) 187–220. https://doi.org/10.1179/imr.1991.36.1.187

[22] D.C. Ramachandran, S.P. Murugan, J. Moon, C.H. Lee,

Y.D. Park, The effect of the hyperstoichiometric Ti/N ratio due to excessive Ti on the toughness of N-controlled novel fire- and seismic-resistant steels, Metallurgical and Materials Transactions A 50 (2019) 3514–3527. https://doi.org/10.1007/s11661-019-05266-1

[23] T. Liu, M.-J. Long, D.-F. Chen, H.-M. Duan, L.-T. Gui, S. Yu, J.-S. Cao, H.-B. Chen, H.-L. Fan, Effect of coarse TiN inclusions and microstructure on impact toughness fluctuation in Ti micro-alloyed steel, Journal of Iron and Steel Research International 25 (2018) 1043–1053. https://doi.org/10.1007/s42243-018-0149-5

[24] A. Ghosh, A. Ray, D. Chakrabarti, C.L. Davis, Cleavage initiation in steel: Competition between large grains and large particles, Materials Science and Engineering: A 561 (2013) 126–135. https://doi.org/10.1016/j.msea.2012.11.019

[25] A.G. Kostryzhev, C.R. Killmore, D. Yu, E.V. Pereloma, Martensitic wear resistant steels alloyed with titanium, Wear 446–447 (2020) 203203. https://doi.org/10.1016/j.wear.2020.203203

[26] Y. Murakami, H. Matsunaga, A. Abyazi, Y. Fukushima, Defect size dependence on threshold stress intensity for high-strength steel with internal hydrogen, Fatigue & Fracture of Engineering Materials & Structures 36 (2013) 836–850. https://doi.org/10.1111/ffe.12077

[27] R. Abushosha, R. Vipond, B. Mintz, Influence of titanium on hot ductility of as cast steels, Materials Science and Technology 7 (1991) 613–621. https://doi.org/10.1179/mst.1991.7.7.613

[28] H. Zhang, Y. Zou, Z. Zou, C. Shi, Effects of chromium addition on microstructure and properties of TiC–VC reinforced Fe-based laser cladding coatings, Journal of Alloys and Compounds 614 (2014) 107–112. https://doi.org/10.1016/j.jallcom.2014.06.073

[29] H. Zhang, Y. Zou, Z. Zou, D. Wu, Microstructures and properties of low-chromium high corrosion-resistant TiC–VC reinforced Fe-based laser cladding layer, Journal of Alloys and Compounds 622 (2015) 62–68. https://doi.org/10.1016/j.jallcom.2014.10.012.

[30] M. Matveeva, Effect of chromium and titanium on structure and properties of white cast iron, Metallurgical and Mining Industry 2(1) (2010) 17–22.

[31] W. Zhuang, H. Zhi, H. Liu, D. Zhang, D. Shi, Effect of titanium alloying on the microstructure and properties of high manganese steel, E3S Web of Conferences 79 (2019). https://doi.org/10.1051/e3sconf/20197901001

[32] J. Chakraborty, D. Bhattacharjee, I. Manna, Austempering of bearing steel for improved mechanical properties, Scripta Materialia 59 (2008) 247–250. https://doi.org/10.1016/j.scriptamat.2008.03.023

[33] Ł. Konat, M. Zemlik, R. Jasiński, D. Grygier, Austenite grain growth analysis in a welded joint of high-strength martensitic abrasion-resistant steel Hardox 450, Materials 14 (2021) 2850. https://doi.org/10.3390/ma14112850

[34] J. Hidalgo, M.J. Santofimia, Effect of prior austenite grain size refinement by thermal cycling on the microstructural features of as-quenched lath martensite, Metallurgical and Materials Transactions A 47 (2016) 5288–5301. https://doi.org/10.1007/s11661-016-3525-4

[35] T. Maki, Morphology and substructure of martensite in steels, Phase Transformations in Steels (2012) 34–58. https://doi.org/10.1533/9780857096111.1.34

[36] S. Morito, H. Tanaka, R. Konishi, T. Furuhara, T. Maki, The morphology and crystallography of lath martensite in Fe-C alloys, Acta Materialia 51 (2003) 1789–1799. https://doi.org/10.1016/s1359-6454(02)00577-3

[37] T. Swarr, G. Krauss, The effect of structure on the deformation of as-quenched and tempered martensite in an Fe-0.2 pct C alloy, Metallurgical Transactions A 7 (1976) 41–48. https://doi.org/10.1007/bf02644037

[38] C. Wang, M. Wang, J. Shi, W. Hui, H. Dong, Effect of microstructural refinement on the toughness of low carbon martensitic steel, Scripta Materialia 58 (2008) 492–495. https://doi.org/10.1016/j.scriptamat.2007.10.053

[39] G. Qiu, D. Zhan, C. Li, Y. Yang, M. Qi, Z. Jiang, H. Zhang, Influence of inclusions on the mechanical properties of RAFM steels via Y and Ti addition, Metals 9 (2019) 851. https://doi.org/10.3390/met9080851

[40] A. Maciejny, Brittleness of Metals, Publishing House "Śląsk", Katowice, 1973.

[41] J.W. Wyrzykowski, E. Pleszakow, J. Sieniawski, Deformation and Cracking of Metals, Publishing House "WNT", Warsaw, 1999.

[42] Kocańda Stanisław, Fatigue Failure of Metals, Publishing House "WNT", Warsaw, 1978.

[43] Y. Prawoto, N. Jasmawati, K. Sumeru, Effect of prior austenite grain size on the morphology and mechanical properties of martensite in medium carbon steel, Journal of Materials Science and Technology 28 (2012) 461–466. https://doi.org/10.1016/S1005-0302(12)60083-8

[44] D. Liu, Z. Wang, J. Liu, Z. Wang, X. Zuo, Study of the fracture behavior of TiN and TiC inclusions in NM550 wear-resistant steel during the tensile process, Metals 12 (2022) 363. https://doi.org/10.3390/met12020363

[45] J. Du, Examination of the effect of TiN particles and grain size on the Charpy impact transition temperature in steels, Journal of Materials Science & Technology 28(10) 2011 878–888. https://doi.org/10.1016/S1005-0302(12)60146-7

[46] J.I. San Martin, J.M. Rodriguez-Ibabe, Determination of energetic parameters controlling cleavage fracture in a Ti-V microalloyed ferrite-pearlite steel, Scripta Materialia 40 (1999) 459–464. https://doi.org/10.1016/s1359-6462(98)00467-9

[47] W. Yan, Y.Y. Shan, K. Yang, Influence of TiN inclusions on the cleavage fracture behavior of low-carbon microalloyed steels, Metallurgical and Materials Transactions A 38 (2007) 1211–1222. https://doi.org/10.1007/s11661-007-9161-2

UTICAJ HROMA I TITANIJUMA NA MIKROSTRUKTURU I MEHANIČKA SVOJSTVA LIVENOG ČELIKA

B. Białobrzeska [a,*], R. Jasiński [a], R. Dziurka [b], P. Bała [b]

[a] Tehnički univerzitet u Vroclavu, Mašinski fakultet, Vroclav, Poljska
[b] AGH Univerzitet u Krakovu, Fakultet za inženjerstvo metala i industrijsku informatiku, Krakov, Poljska

Apstrakt

U ovom radu istražen je uticaj hroma i titanijuma na mikrostrukturu i mehanička svojstva livenog čelika. Analiza je sprovedena na materijalu pokrivenom patentom Pat.243157. Korišćene su napredne tehnike, uključujući dilatometrijsku analizu, svetlosnu mikroskopiju (LM), skenirajuću elektronsku mikroskopiju (SEM) i transmisionu elektronsku mikroskopiju (TEM). Materijal je ispitan u različitim stanjima: kao liv, kaljen, te kaljen sa naknadnim žarenjem na 200 °C, 400 °C i 600 °C. Ispitana su važna mehanička svojstva poput tvrdoće, napona tečenja, procenta izduženja, procenta smanjenja površine nakon loma i udarne žilavosti pri temperaturama od -40 °C do +20 °C. Rezultati su upoređeni sa referentnim livenim čelikom bez ovih legirajućih elemenata, što je omogućilo detaljnu procenu uticaja hroma i titanijuma. Istraživanje započinje sveobuhvatnim pregledom literature o uticaju ovih elemenata na legure na bazi železa. Rezultati ističu uticaj hroma i titanijuma na mehanička svojstva i mikrostrukturni razvoj livenog čelika. Pokazano je da ovi elementi igraju ključnu ulogu u poboljšanju mehaničke čvrstoće, naročito nakon kaljenja i žarenja, iako su kompromisi u pogledu duktilnosti i udarne žilavosti očigledni. Pored toga, u radu se diskutuje o mehanizmima oštećenja, sa posebnim osvrtom na ulogu titanijumovih nitrida u procesu pucanja.

Ključne reči: *Liveni čelik; Titanijum, Hrom; Termička obrada; Mikrostruktura; Mehanička svojstva*